Deep Space Network

203
Sequential Ranging

Document Owner:		Approved by:	
Signature Provided	06/20/2019	Signature Provided	06/13/2019
Andrew O'Dea Telemetry, Tracking, and Command System Engineer	Date	Timothy Pham Communications Systems Chief Engineer	Date
Prepared By:		**Released by:**	
Signature Provided	06/13/2019	Signature Provided	06/20/2019
Peter Kinman Telecommunications Technical Consultant	Date	Christine Chang DSN Document Release Authority	Date

DSN No. **810-005, 203, Rev. D**
Issue Date: July 17, 2019
JPL D-19379; CL# 19-4107

Jet Propulsion Laboratory
California Institute of Technology

Users must ensure that they are using the current version in DSN Telecommunications Link Design Handbook website:
https://deepspace.jpl.nasa.gov/dsndocs/810-005/

Review Acknowledgment

By signing below, the signatories acknowledge that they have reviewed this document and provided comments, if any, to the signatories on the Cover Page.

Signature Provided	06/13/2019	Signature Provided	06/18/2019
Jeff Berner DSN Project Chief Engineer	Date	Scott Bryant DSN Ranging Cognizant Development Engineer	Date

Document Change Log

Rev	Issue Date	Prepared By	Affected Sections or pages	Change Summary
Initial	1/15/2001	P. W. Kinman	All	New Module
A	2/20/2006	P. W. Kinman	Many	Revised to incorporate changes resulting from improvements in sequential ranging implementation.
B	4/2/2007	P. W. Kinman	2.6	Added new paragraph in section on “Range Measurement Performance” providing recommended range for P_r/N_0.
C	10/31/2009	P. W. Kinman	Page 5, 31, 40, A1 & A2	Removed references of the 26-m subnet stations for they have been decommissioned. Made editorial changes.
D	07/17/2019	P. W. Kinman	Many	Rewrote “Allocation of Link Power” section, including new models for downlink phase deviation for each of two types of ranging channels. Reorganized “Range Measurement Performance” section, including new curve fit and new interpolation for probability of acquisition. Removed square-wave models. Added glossary. Rewrote many paragraphs for improved clarity.

Contents

Illustrations

Figure **Page**

Tables

Table **Page**

1. Introduction

1.1 Purpose

This module describes capabilities of the Deep Space Network (DSN) for sequential ranging. These capabilities are available within the 70-m, the 34-m High Efficiency (HEF), and the 34-m Beam Waveguide (BWG) subnets.

1.2 Scope

The material contained in this module covers the sequential ranging system that may be utilized by both near-Earth and deep-space missions. This document describes those parameters and operational considerations that are independent of the particular antenna being used to provide the telecommunications link. For antenna-dependent parameters, refer to Module 101, 103, or 104 of this handbook. The other ranging scheme employed by the DSN is PN ranging, described in Module 214.

An overview of the ranging system is given in Section 2.1. The sequential ranging signal structure is explained in Section 2.2. The parameters to be specified for ranging operations are explained in Section 2.3. The distribution of link power is characterized in Section 2.4. The spectrum of an uplink carrier modulated by a sequential ranging signal is described in Section 2.5. The performance of sequential ranging is summarized in Section 2.6. In Section 2.7 the corrections required to determine the actual range to a spacecraft are described. In Section 2.8 the total error for a range measurement is discussed.

2. General Information

The ranging signal of interest in this module is a sequence of periodic signals; this signaling technique is called sequential ranging. A different signaling technique, PN ranging, is also supported by the DSN. The same instrumentation within the DSN supports both sequential ranging and PN ranging. However, there are performance differences between these two signaling techniques. This module only discusses sequential ranging. PN ranging is discussed in Module 214.

The range clock is coherently related to the carrier. The uplink carrier is often tuned during a tracking pass, in order to compensate for the Doppler effect on the uplink carrier, thereby reducing stress on the transponder's carrier-tracking loop. As the uplink carrier is tuned, the range-clock frequency varies proportionately.

In two-way ranging, one Deep Space Station (DSS) both transmits the uplink and receives the downlink. For two-way ranging, the user may calculate the round-trip light time (RTLT) from data provided by the DSN: phase measurements of the ranging signal and a record of the transmitted uplink carrier frequency.

Three-way ranging is also supported, for which one DSS transmits the uplink and a different DSS receives the downlink. As with two-way ranging, the DSN reports phase measurements of the ranging signal and a record of the uplink-carrier frequency. From these

data, the user may calculate the light time for the travel of the ranging signal from the uplink DSS, through the spacecraft, to the downlink DSS.

To put matters in perspective, the measurements discussed here are phase measurements and the resulting data permit the user to calculate time delays. Range cannot be calculated directly and accurately from the time delays because the range changes significantly over the course of the signal travel time. Similar measurement techniques employed in terrestrial applications, where the distances and measurement times are much smaller, typically permit the calculation of the range as the two-way time delay times the speed of an electromagnetic wave divided by 2. That has been the justification for using the term range measurement for this class of measurement technique. The two-way and three-way time delays calculated for deep-space missions are useful in the orbit determination process. These calculated delays assist in the improvement of trajectory models; and so, indirectly, the delays assist in the estimation of range as a function of time.

It is customary to quote range measurement error in units of meters. For two-way ranging, the range error is defined as the error in the two-way time delay times the speed of electromagnetic waves in vacuum divided by 2. (The division by two accounts for the fact that range is a one-way distance but the time delay is two-way.)

2.1 System Description

The DSN ranging system records the phase of the ranging signal that is transmitted and measures the phase of the ranging signal that returns. For two-way ranging, both recorded phase values (that of the uplink ranging signal and that of the downlink ranging signal) apply to a common instant in time, an epoch of the 1-pulse per second timing reference, which becomes the common time tag. From the difference between the uplink and downlink phases and from the history of the transmitted range-clock frequency (which can be calculated from the history of the uplink-carrier frequency), a user may compute the RTLT (Reference 1). This two-way time delay applies to a signal arriving at the DSS at the instant specified by the time tag.

The architecture for the DSN ranging system is shown in Figure 1. The ranging signal originates in the Uplink Subsystem (UPL). The returned signal is processed in the Downlink Tracking and Telemetry Subsystem (DTT). Both the UPL and the DTT are located at the Deep Space Communications Complex (DSCC).

The signal processing in the UPL may be summarized as follows. The Uplink Signal Generator (USG) synthesizes the range clock such that it is coherently related to the uplink carrier. The range-clock frequency equals a rational factor times the uplink carrier frequency. The USG generates the ranging signal, which is the range clock modified by additional signal structure that makes possible resolution of the phase ambiguity. A sample of the uplink phase, which is required for the delay measurement, is passed from the USG to the Uplink Processor Assembly (UPA). The USG modulates the uplink carrier with the ranging signal. The klystron supplies the final stage of power amplification for the uplink carrier.

The downlink carrier, after amplification within the Low-Noise Amplifier (LNA), passes to the DTT. Frequency down-conversion to an intermediate frequency (IF) takes place in the RF-to-IF Downconverter (RID). The IF signal is sent to an IF-to-Digital Converter (IDC). Demodulation of the IF carrier occurs in the Receiver, Ranging and Telemetry (RRT) processor.

Also within the RRT, the correlation of the received, baseband ranging signal with a local model produces a measurement of the downlink phase. This downlink phase is passed to the Downlink Channel Controller (DCC).

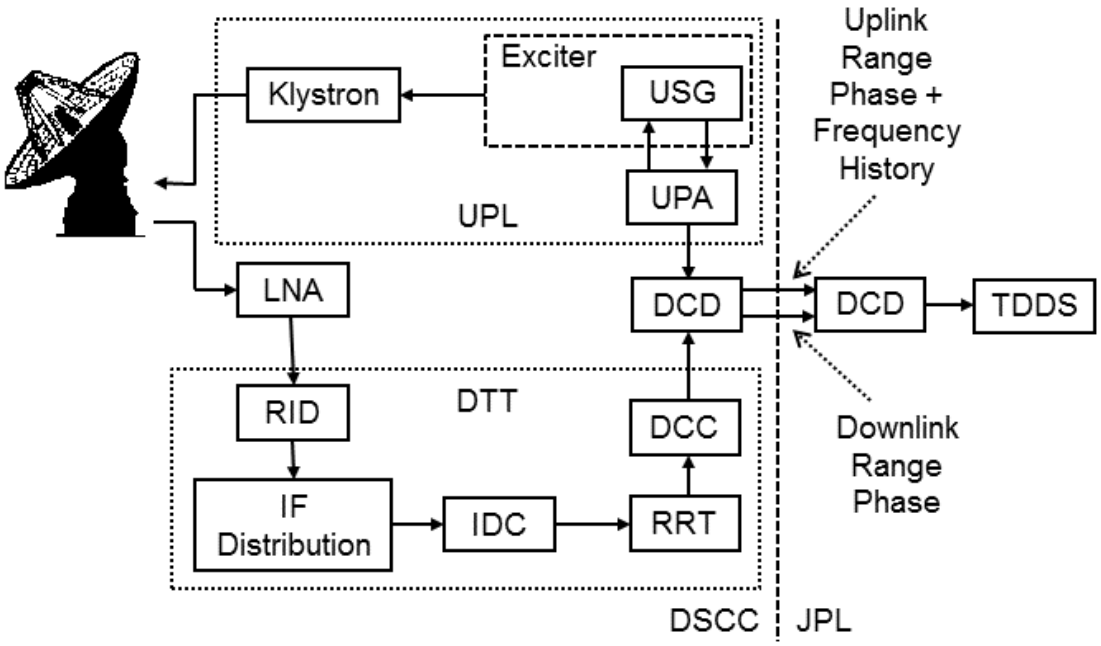

Figure 1. The DSN Ranging System Architecture

Uplink phase samples, each corresponding to an epoch of the 1-PPS (pulse per second) clock, are passed from the UPA, via the Data Capture and Delivery (DCD) software, to the Tracking Data Delivery Subsystem (TDDS), located in Pasadena. The DCC passes the downlink phase measurement and its time tag (an epoch of the 1-PPS clock), via the DCD, to the TDDS. A history of the uplink range clock's frequency is also needed for the calculation of the two-way time delay. Since the uplink range clock is coherently related to the uplink carrier, this necessary information can be derived from the history of the uplink carrier frequency, which is supplied by the UPA to the TDDS. All data required for the two-way delay calculation are archived by the TDDS for later use by a navigation team or other users.

The IDC, RRT, and DCC required for the processing of a downlink carrier are located within a Downlink Channel Processing Cabinet (DCPC). Each DCPC supports a single channel. For spacecraft with multiple channels (for example, X-band and Ka-band), or for multiple spacecraft within a single antenna beamwidth, multiple DCPCs will be assigned to that antenna.

The DSN uses the Range Unit (RU) to deliver the difference of the ranging signal's uplink phase and downlink phase. Since the range clock and the carrier are coherently related, it is permissible to define the RU in terms of carrier phase. For an S-band uplink, the RU is defined as two cycles of the carrier. For an X-band uplink, one RU is $(749/221)$ times two cycles of the carrier. For a Ka-band uplink, one RU is $(3599/221)$ times two cycles of the

carrier. Because the RU is defined with a factor (1 for an S-band uplink, $749/221$ for an X-band uplink, and $3599/221$ for a Ka-band uplink) that is proportional to frequency, the RU is proportional to time delay. (But the RU is a dimensionless unit.) One RU corresponds to approximately 0.94 ns of time delay.

A user may convert a two-way phase delay in RU into a two-way time delay as follows:

$$\text{Two-way Time Delay} = \begin{cases} \dfrac{2 \times RU}{f_S}, & \text{S-band uplink} \\ \dfrac{749}{221} \cdot \dfrac{2 \times RU}{f_X}, & \text{X-band uplink} \\ \dfrac{3599}{221} \cdot \dfrac{2 \times RU}{f_{Ka}}, & \text{Ka-band uplink} \end{cases} \quad (1)$$

where f_S is the frequency of an S-band uplink carrier, f_X is the frequency of an X-band uplink carrier, and f_{Ka} is the frequency of a Ka-band uplink carrier. For example, if the uplink carrier is in the X band with a frequency of 7.16 GHz and the two-way phase delay is reported as 6,500,000 RU, then the two-way time delay is 6,153,467 ns.

2.2 Sequential Ranging Signal Structure

The sequential ranging signal is a sequence of periodic signals. These periodic signals are all coherently related to each other and to the uplink carrier. The basis for these periodic ranging signals is a table of well-defined range components.

2.2.1 Range Components

The range components are periodic signals. Each component is assigned a number. A larger number represents a component with a smaller frequency (but a larger period). The components that are available, at least in theory, are ordered according to these component numbers. The frequency f_0 of component 0, which is never actually used in practice, is related to the uplink carrier frequency by

$$f_0 = \begin{cases} 2^{-7} \cdot f_S\,, & \text{S-band uplink} \\ 2^{-7} \cdot \dfrac{221}{749} \cdot f_X\,, & \text{X-band uplink} \\ 2^{-7} \cdot \dfrac{221}{3599} \cdot f_{Ka}\,, & \text{Ka-band uplink} \end{cases} \quad (2)$$

where f_S is the frequency of the S-band uplink carrier, f_X is the frequency of the X-band uplink carrier, and f_{Ka} is the frequency of the Ka-band uplink carrier. The frequency f_n of component n is related to f_0 by

$$f_n = 2^{-n} \cdot f_0 \quad (3)$$

Because the component frequencies are related to the uplink carrier frequency, the exact values of the component frequencies depend on the channel assignment and any uplink Doppler compensation that may be present. An example table of the transmitted range component frequencies is given in Table 1 for channel assignment 18, assuming the transmitted

uplink carrier is at its nominal channel frequency (no uplink Doppler compensation). The frequencies of Table 1 are rounded-off to the nearest millihertz. (In a typical measurement, the component frequencies are known to a better accuracy than 1 mHz. The intent of Table 1 is to give the reader a general idea of the component frequencies and how they vary with component number.) Even though Table 1 represents a particular case (nominal Channel 18), there are discernable features of this table that are also present in any table of range component frequencies. The frequency of component 4 is always approximately 1 MHz, and it is often called the "1 MHz component". Every component has a frequency that is exactly half of its immediate predecessor.

Whenever a periodic signal is used to measure signal delay, there is an ambiguity. The phase delay consists, in principle, of an integer number of cycles plus some fraction of a cycle. If only one periodic signal of frequency f_n is used in the measurement, only the fractional part of the phase delay (a fraction of one cycle) can be measured. The integer number of cycles in the delay cannot be known from the measurement itself. However, *a priori* knowledge of the approximate value of the delay may provide that information. The successful resolution of the ambiguity requires that the *a priori* estimate of the delay be correct to within 1 cycle of phase. In time units, the *a priori* estimate of the delay must be correct to within 1 period ($1/f_n$). Considering that the speed c of an electromagnetic wave in vacuum is 299,792,458 m/s and that the delay measurement is two-way, the *a priori* estimate of the range must be correct to within $c/(2\,f_n)$ if the ambiguity is to be resolved. This is the number entered in the third column of Table 1.

2.2.2 Range Clock

The first periodic signal in the ranging sequence is called the range clock. With component n_{RC} as the range clock, the frequency f_{RC} of the range clock is

$$f_{RC} = \begin{cases} (2^{-7-n_{RC}}) \cdot f_S\,, & \text{S-band uplink} \\ (2^{-7-n_{RC}}) \cdot \dfrac{221}{749} \cdot f_X\,, & \text{X-band uplink} \\ (2^{-7-n_{RC}}) \cdot \dfrac{221}{3599} \cdot f_{Ka}\,, & \text{Ka-band uplink} \end{cases} \tag{4}$$

This equation is consistent with Equations (2) and (3).

2.2.3 Ranging Sequence

The ranging signal consists of a sequence of range components. The first is the range clock. The second is the component having a component number equal to one plus that of the range clock. The third is the component having a component number equal to two plus that of the range clock, and so forth. For example, if the range clock is component 4, then the sequence is 4, 5, 6, etc.

All range components in a ranging sequence except the first (the range clock) are known as ambiguity-resolving components. The number of ambiguity-resolving components that should be used in the ranging sequence for any particular range measurement is determined by the required ambiguity-resolving capability for that measurement. The range components

always occur sequentially, in order of increasing component number, without skipping any, from the range clock to the last ambiguity-resolving component.

Table 1. Range Components for Channel 18 (Nominal)

Component Number	Frequency (Hz)	Ambiguity-Resolving Capability (km)
4	1,032,556.981	0.1452
5	516,278.490	0.2903
6	258,139.245	0.5807
7	129,069.623	1.1614
8	64,534.811	2.3227
9	32,267.406	4.6454
10	16,133.703	9.2909
11	80,66.851	18.5818
12	4,033.426	37.1635
13	2,016.713	74.3270
14	1,008.356	148.6540
15	504.178	297.3081
16	252.089	594.6161
17	126.045	1,189.2323
18	63.022	2,378.4645
19	31.511	4,756.9291
20	15.756	9,513.8581
21	7.878	19,027.7163
22	3.939	38,055.4326
23	1.969	76,110.8651
24	0.985	152,221.7303

In any given measurement, some ambiguity-resolving components will be multiplied by a higher-frequency component; this multiplication is called chopping. The purpose of chopping is to enforce spectral separation between the ranging signal and command on the uplink and between the ranging signal and telemetry on the downlink. The effect of the chopping is to modulate the lower frequency range components onto a ranging subcarrier. This ranging subcarrier is called the chop component. Often, the chop component is the range clock. Figure 2 shows an example of component 6 multiplied (chopped) by component 4. In this case, the chop component 4 has a frequency four times that of component 6, so there are two cycles of the chop component for each half-cycle of component 6. The user specifies at which point in the sequence the chopping should begin; all components after this point are multiplied by the chop component. The user also specifies the chop component. This chop component remains the same for the duration of the range measurement session.

The ranging sequence passes through the uplink ranging filter on its way to the phase modulator for the uplink carrier. This filter, implemented digitally in the USG, is low-pass with a default bandwidth of 1.2 MHz but is configurable for larger bandwidths. The purpose of the uplink ranging filter is to reduce the bandwidth of the modulated carrier for the sake of spectral efficiency. In Figure 2, the chop component (component 4, in this case) is shown as a sinewave; this is a good approximation when the uplink ranging filter passes the fundamental harmonic of the range clock but blocks the third and higher-order harmonics.

The purpose of ranging with a sequence is to get the advantages of both high-frequency and low-frequency range components. The accuracy of a range measurement improves when a higher-frequency range clock is used (see Section 2.6). All components that follow the range clock are present in order to resolve the phase ambiguity. The ambiguity-resolving capability of a ranging sequence equals the ambiguity-resolving capability of the lowest-frequency range component (see, for example, Table 1).

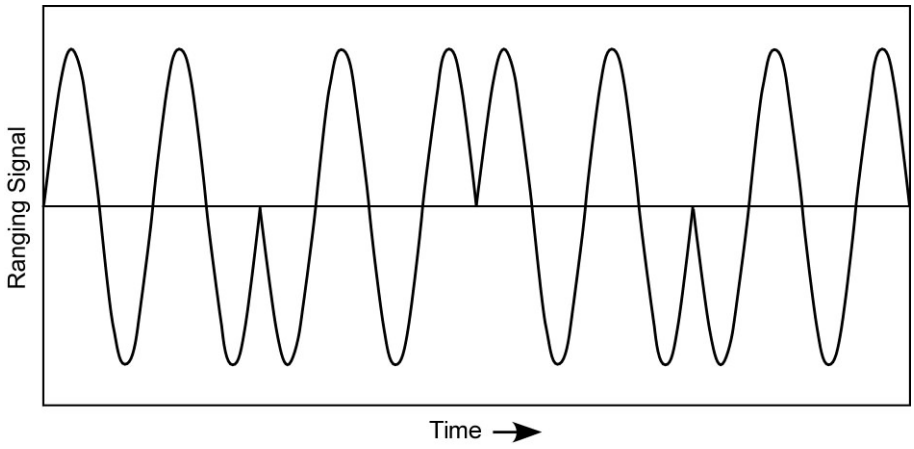

Figure 2. Component 6 Chopped by Sinewave Component 4

2.2.4 Sequence Timing

Three parameters control the timing of the transmitted sequence: the transmit time (XMIT), the integration time T_1 that is to be used for the range clock, and the integration time T_2 that is used to be used for each of the ambiguity-resolving components. XMIT is always selected to fall on an integer-second epoch, as determined by the uplink timing system. That is to say, this time, when expressed in seconds, has no fractional part. Each of the integration times T_1 and T_2 is an integer number of seconds.

2.2.4.1 Timing at the Exciter

At the exciter, the actual start time of the ranging sequence, which is also the start time of the range clock, is 1 second before the specified time XMIT. (The purpose of this slightly early start is to increase the probability that the range clock integration at the receiver does not begin before the range clock arrives at the receiver.) The range clock persists from the $(\text{XMIT} - 1)$-second epoch up through the $(\text{XMIT} + T_1 + 1)$-second epoch. The transition from the range clock to the first ambiguity-resolving component occurs sometime within the 1-second interval that immediately follows the $(\text{XMIT} + T_1 + 1)$-second epoch. Hence, the range clock is present for $T_1 + 2$ seconds (plus a fraction of another second).

Once the first ambiguity-resolving component has started, a fraction of a second before the $(\text{XMIT} + T_1 + 2)$-second epoch, it persists up through the $(\text{XMIT} + T_1 + T_2 + 2)$-second epoch. The transition to the next ambiguity-resolving component occurs sometime within the 1-second interval that immediately follows the $(\text{XMIT} + T_1 + T_2 + 2)$-second epoch. Hence, the first ambiguity-resolving component has a duration of at least T_2. The actual duration is typically about $T_2 + 1$ seconds: from a fraction of a second before the $(\text{XMIT} + T_1 + 2)$-second epoch to a fraction of a second after the $(\text{XMIT} + T_1 + T_2 + 2)$-second epoch, but no guarantee is made for a duration longer than T_2.

In general, the transition to the *n*-th ambiguity-resolving component occurs a fraction of a second before the $[\text{XMIT} + T_1 + 2 + (n-1) \cdot (T_2 + 1)]$-second epoch. The duration of the *n*-th ambiguity-resolving component is typically about $T_2 + 1$ seconds, but no guarantee is made for a duration longer than T_2.

Figure 3 shows an example of the sequence timing. In this example, the range clock is component 4 (C4) and the last component is 9 (C9). The range clock begins 1 second before XMIT. After XMIT, the range clock continues for an additional T_1 seconds (for the nominal measurement) plus 1 second (as a margin for error). During the next second there is a transition from the range clock to component 5 (C5). The transition itself occurs essentially instantaneously, but there is no programmatic guarantee of when within this second the actual transition occurs. There is another transition second following the planned T_2-second period for C5. The pattern established by C5 is repeated for components 6 through 9 (C6 through C9). Following a transition second that accommodates the transition from C9 back to C4 (in preparation for a second range measurement), the range clock is transmitted for 1 second (as a margin for error) plus T_1 seconds (for the nominal measurement), and so forth.

The phase is continuous throughout the ranging sequence, including at the transitions from one component to the next. This is essential for the correct resolution of the phase ambiguity.

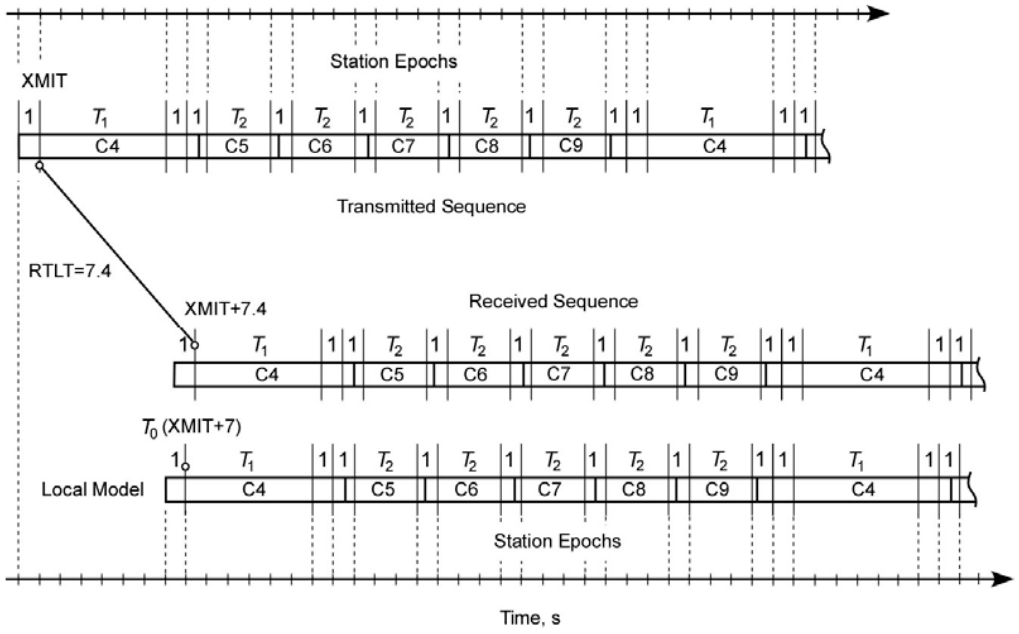

Figure 3. Example Timing Diagram
$T_1 = 6$ s, $T_2 = 3$ s, RTLT = 7.4 s

2.2.4.2 Timing at the Receiver

At the receiver, the estimated RTLT is an input parameter. Within the DTT this estimate is rounded-off to the nearest integer second. The rounded-off, estimated RTLT is added to XMIT to get the start time T_0 of the range-clock integration. The start time T_0, when expressed in seconds, has no fractional part. The range clock integration extends from the T_0 epoch to the $T_0 + T_1$ epoch, as marked by the timing system. The error introduced to T_0 by round-off is no larger than 0.5 second. Therefore, if the estimated RTLT is correct to within 0.5 second, T_0 is different from XMIT + RTLT by less than 1 second. That is why the range clock at the exciter begins 1 second before the specified sequence start time and ends $T_1 + 1$ seconds after the specified start time. The 1-second padding at the start and at the end of the range clock interval ensures that the range clock is present at the receiver during the entire range clock integration (as long as the estimated RTLT is correct to within 0.5 second).

The integration for the first ambiguity-resolving component begins at the $(T_0 + T_1 + 2)$-second epoch. Hence, there is 2-second interval that separates the range-clock integration from that of the first ambiguity-resolving component.

In general, the integration for the n-th ambiguity-resolving component begins at the $[T_0 + T_1 + 2 + (n-1) \cdot (T_2 + 1)]$-second epoch. There is a 1-second interval that separates the integrations of any two ambiguity-resolving components.

Figure 3 is an example of the timing. In this example, the RTLT (and the estimated RTLT) is 7.4 s. This value is rounded-off to 7 s within the DTT. In this case, T_0 is less than XMIT + RTLT by 0.4 s. Shown in Figure 3 is the received sequence as well as a local

model of that sequence, as computed from T_0. The local model is, in this case, 0.4 s in advance of the received sequence. The timing of the component integrations is determined by this local model. In this case, all integrations begin 0.4 s early.

Because T_0 does not, in general, exactly equal XMIT + RTLT, it will sometimes happen that the integration of each ambiguity-resolving component in a range measurement begins slightly before that component arrives or ends slightly after that component departs. In such cases, the effective integration time for each ambiguity-resolving component is slightly less than the design value T_2. The difference between the design value and the effective value of T_2 is typically a fraction of a second. Normally, this is not a problem. However, if the design value T_2 is only 1 or 2 seconds, the degradation in performance may be noticeable, as discussed in Subsection 2.6.5.1. As mentioned previously, this alignment problem does not affect the range-clock integration (as long as the estimated RTLT is correct to within 0.5 s), owing to the 1-s padding at the start and the end of the range clock interval.

2.2.4.3 Cycle Time

Typically, range measurements are done serially during a tracking pass. For each range measurement there is a ranging sequence of the type described above (a range clock followed by a set of ambiguity-resolving components). When the ranging sequence associated with one range measurement ends, another ranging sequence with exactly the same signal structure begins immediately. The cycle time is the repetition period of the range measurements. The cycle time is given by

$$\text{Cycle Time} = T_1 + 3 + (n_L - n_{RC}) \cdot (T_2 + 1) \quad \text{seconds} \tag{5}$$

where n_L is the range component number of the last ambiguity-resolving component and n_{RC} is the range component number of the range clock. In light of the previous discussion of sequence timing, Equation (5) can be understood as follows. There is a period of time, $T_1 + 2$ seconds, during which the range clock is transmitted, followed by a 1-second interval that contains the transition from the range clock to the first ambiguity-resolving component. This is the $T_1 + 3$ seconds appearing in Equation (5). There are $(n_L - n_{RC})$ ambiguity-resolving components. Each of these ambiguity-resolving components has a guaranteed duration T_2, and associated with each ambiguity-resolving component is a 1-second interval that contains the transition to the next component.

The last component n_L should be chosen carefully if it is desirable to maximize the number of range data points in a tracking pass. For any given *a priori* range ambiguity, there is a minimum n_L that will resolve the ambiguity (see Table 1). Choosing an n_L larger than this will reduce the number of range data points that can be obtained in a tracking pass. Table 2 shows the number of range points that can be obtained per hour as a function of n_L for integration time $T_1 = 100$ s and for range clock component $n_{RC} = 4$.

Table 2. Range Points per Hour

$T_1 = 100$ s and $n_{RC} = 4$

n_L	Range Points per Hour	
	$T_2 = 5$ s	$T_2 = 20$ s
12	23.8	13.3
13	22.9	12.3
14	22.1	11.5
15	21.3	10.8
16	20.6	10.1
17	19.9	9.6
18	19.3	9.1
19	18.7	8.6
20	18.1	8.2
21	17.6	7.8
22	17.1	7.5
23	16.6	7.2
24	16.1	6.9

2.3 Parameters Specified for Ranging Operations

The following subsections present the parameters that are required in ranging operations.

2.3.1 Ranging Sequence Parameters

The ranging sequence is established by specifying the range clock component number, the last component number, the chop component number, the component number at which chopping begins, and the integration times T_1 and T_2.

The range clock component number determines the approximate frequency of the range clock. The exact frequency of the range clock is set by its relation to the uplink carrier frequency (see Section 2.2). The range clock is typically selected to be component 4, which corresponds to a range-clock having a frequency of approximately 1 MHz.

The last component number determines the ambiguity-resolving capability of the ranging sequence. Therefore, the proper selection of this number depends on *a priori* knowledge of the range. The approximate ambiguity-resolving capability of the different range components is given in Table 1. The exact ambiguity-resolving capability depends on the uplink frequency.

The purpose of chopping is to enforce spectral separation between the ranging sequence and the command signal on the uplink and between the ranging sequence and the telemetry signal on the downlink. Selection of the chop component and the component at which chopping begins should be made with this in mind.

There is a fundamental trade-off in the selection of the integration times T_1 and T_2. On the one hand, a large T_1 decreases the range measurement error due to thermal noise and a large T_2 increases the probability of range acquisition (see Section 2.6). On the other hand, large values for T_1 and T_2 increase the cycle time (see Section 2.2), decreasing the number of range measurements that can be made in a tracking pass. The selection of these integration times will depend on the available the ratio P_R/N_0 of the downlink ranging signal power to the noise spectral density (see Section 2.6).

2.3.2 Correlation Type

Either a sinewave or a squarewave may be used at the receiver as the local model of the range clock for the purpose of correlation. Normally, the user will select a local model that matches the form of the actual range clock. A small degradation in performance results if a local model is selected that does not match the form of the actual range clock.

2.3.3 Uplink Ranging Modulation Index

The uplink ranging modulation index is chosen to get a suitable distribution of power among the ranging and command sidebands and the residual carrier on the uplink (see Section 2.4). The uplink ranging modulation index also affects the distribution of power on the downlink carrier, because of the turn-around processing in the spacecraft transponder. The analysis appearing below employs an rms phase deviation of the uplink carrier. This rms phase deviation equals the peak modulation index divided by $\sqrt{2}$ for the case of a sinewave range clock.

2.3.4 Probability of Acquisition Tolerance

The tolerance plays a role in deciding whether to judge range acquisitions as "in lock" or "out of lock". The ranging process does not use a phase-locked loop, so ranging lock status is estimated using the ranging probability of acquisition. For any given range acquisition, the ratio P_R/N_0 of the downlink ranging signal power to the noise spectral density is measured. From this measured P_R/N_0, an estimate of the probability of acquisition P_{acq} is calculated. Section 2.6 describes the calculation of the P_{acq} from P_R/N_0.

Tolerance may be selected over the range of 0.0% to 100.0%. The default value for tolerance is 99%. An acquisition lock status depends upon the following criteria:

$P_{\text{acq}}(\%) \geq \text{Tolerance}$ *results in* Acquisition declared "in lock"

$P_{\text{acq}}(\%) < \text{Tolerance}$ *results in* Acquisition declared "out of lock"

This procedure is explained for the example where the tolerance has the default value of 99%. For a given acquisition, P_R/N_0 is measured. From this measured value, the probability of acquisition P_{acq} is calculated; this number is the probability that the ambiguity is correctly resolved for this particular acquisition. Treating P_{acq} as a percentage, it is compared with the tolerance of 99%. If $P_{\text{acq}}(\%)$ equals or exceeds 99%, the acquisition is declared "in lock". Otherwise, it is declared "out of lock". Note that the "out of lock" ranging data may be valid data, with a probability of $P_{\text{acq}}(\%)$ of being correct.

2.4 Allocation of Link Power

The power allocation for a link is the distribution of power among the important link components: the residual carrier, the ranging sidebands, and the data (command or telemetry) sidebands. The following notation is used here for both the uplink and downlink:

P_C = power in residual carrier

P_R = usable power in ranging sidebands

P_D = usable power in data sidebands

P_T = total link power

P_C is the power in a single spectral line at the carrier frequency. When P_C is finite (greater than zero), carrier synchronization may be obtained at the receiver using a phase-locked loop that tracks this residual carrier. (Carrier synchronization may also be obtained with a Costas loop tracking the data sidebands, which are symmetrically located about the nominal carrier frequency.)

P_R is that portion of the power in the ranging sidebands that is used in the range measurement. At the beginning of the ranging sequence, when the range clock is present, P_R comprises two discrete spectral lines (one at f_{RC} Hz above and a second at f_{RC} Hz below the residual carrier) that correspond to the range clock's fundamental harmonic. Higher-order harmonics (beyond the fundamental harmonic) of the range clock are not used in a range measurement and are not included in P_R. For the components in the ranging sequence that come after the range clock, P_R comprises those discrete spectral lines, both above and below the residual carrier, that correspond to the fundamental harmonic of the component or of the chop component.

For the uplink, P_D is that portion of the power in the command sidebands that is employed in command detection in the transponder. In the most common signal design for a deep-space uplink, command data modulate a sinewave subcarrier and P_D only accounts for the power in the sidebands associated with the upper and lower fundamental harmonic of the subcarrier frequency. In the case of a sinewave subcarrier, the higher-order harmonics of the subcarrier frequency are not employed in command detection in the typical transponder and are not included in P_D.

For some missions, the command signal is bi-polar. An example of this is when the command symbols, represented as rectangular pulses, directly phase-modulate the uplink carrier. In this case, the uplink P_D accounts for all power in command sidebands, since the

command detection process in the typical transponder utilizes all command sidebands arising from a bi-polar command signal.

For the downlink, P_D is that portion of the power in the telemetry sidebands that is employed in telemetry detection at the station. Commonly, the telemetry signal is bi-polar; this happens when rectangular pulses (the telemetry symbols) directly phase-modulate the downlink carrier or when these symbols modulate a square-wave subcarrier that, in turn, phase-modulates the downlink carrier. In such cases, all of the power in the telemetry sidebands is employed in telemetry detection. This is a result of both the data and the subcarrier (if present) being bi-polar.

For some missions, the telemetry signal modulates a sinewave subcarrier and this composite signal phase-modulates the downlink carrier. In such a case, the downlink P_D is that portion of the power in the telemetry sidebands that is employed in telemetry detection at the station. Not included is the power in the higher-order harmonics of the subcarrier frequency.

P_T is not, in general, the sum of P_C, P_R, and P_D. In general, P_T is larger than that sum. There are multiple reasons for this. First, P_R does not account for power in the higher-order harmonics of a sinewave range clock. Second, when multiple signals (for example, a ranging signal and a telemetry signal) simultaneously phase-modulate a carrier, intermodulation products arise. These intermodulation products consume link power but do not contribute to either the range measurement or telemetry detection. Moreover, for the downlink, noise sidebands are present (in the case of turn-around ranging).

In calculating power allocations for a modulated carrier, it is necessary to characterize the level of the modulation. In this document, the root-mean-square (rms) phase deviation of the carrier will be used for this purpose. The following symbols are used in this module to represent rms phase deviation of the carrier:

uplink:	ϕ_r	=	rms phase deviation by ranging signal, rad rms
uplink:	ϕ_{cmd}	=	rms phase deviation by command signal, rad rms
downlink:	θ_{rs}	=	rms phase deviation by ranging signal (strong signal), rad rms
downlink:	θ_r	=	rms phase deviation by ranging signal, rad rms
downlink:	θ_{cmd}	=	rms phase deviation by feedthrough command signal, rad rms
downlink:	θ_n	=	rms phase deviation by noise, rad rms
downlink:	θ_{tlm}	=	rms phase deviation by telemetry signal, rad rms

On the uplink, ϕ_r and ϕ_{cmd} are parameters, constant for any given tracking pass. For a sinewave range clock, ϕ_r is related to the peak modulation index for uplink ranging by:

$$\phi_r = (\text{peak modulation index for uplink ranging, rad})/\sqrt{2} \tag{6}$$

When a sinewave subcarrier is used with command, ϕ_{cmd} is related to the peak modulation index for command by:

$$\phi_{cmd} = (\text{peak modulation index for command, rad})/\sqrt{2}, \quad \begin{matrix}\text{sinewave}\\ \text{subcarrier}\end{matrix} \tag{7}$$

However, for a bi-polar command signal, ϕ_{cmd} equals the peak modulation index for command.

A turn-around ranging channel is used for sequential ranging. Within this channel the uplink carrier is demodulated, and the baseband signal plus noise that is the result of this demodulation is presented to a filter. The filter output is applied to an automatic gain control (AGC) circuit. The signal plus noise that exits the turn-around ranging channel is phase-modulated onto the downlink carrier.

On the downlink, θ_{rs} is a constant parameter that is determined by the AGC in the turn-around ranging channel. θ_{rs} is the rms phase deviation of the downlink carrier by the ranging signal in a strong-signal scenario. In such a scenario, the noise in the transponder's ranging channel is negligible compared with the ranging signal and there is no command. This scenario occurs in a test facility before flight and in the early phase of flight when the ranging signal-to-noise ratio in the transponder's ranging channel is large. For a sinewave range clock, θ_{rs} is related to the peak modulation index (strong signal) by:

$$\theta_{rs} = (\text{strong-signal peak modulation index for downlink ranging, rad})/\sqrt{2} \qquad (8)$$

For an arbitrary signal-to-noise ratio in the transponder's ranging channel, the rms phase deviation by ranging signal on the downlink, denoted θ_r, is less than or equal to θ_{rs}. Thus, θ_r is a variable, depending on both the parameter θ_{rs} and the ranging signal-to-noise ratio in the ranging channel. θ_{rs} is the limiting value of θ_r, corresponding to the strong-signal case. If command is present on the uplink and that command passes through the transponder's ranging channel, then θ_r also depends on the command signal-to-noise ratio in the ranging channel.

Uplink noise passes through the ranging channel and is phase-modulated onto the downlink carrier. θ_n is the rms phase deviation by this ranging-channel noise. θ_n, like θ_r, is a variable that depends on both the parameter θ_{rs} and the ranging signal-to-noise ratio (and, possibly, also the command signal-to-noise ratio) in the ranging channel.

θ_{tlm} is the rms phase deviation of the downlink carrier due to telemetry. When the telemetry signal is bi-polar, the rms phase deviation and the peak modulation index for telemetry are identical. When a sinewave subcarrier is used with telemetry, θ_{tlm} is related to the peak modulation index for telemetry by:

$$\theta_{tlm} = (\text{peak modulation index for telemetry, rad})/\sqrt{2}, \quad \begin{matrix}\text{sinewave}\\ \text{subcarrier}\end{matrix} \qquad (9)$$

2.4.1 Uplink

The equations of this subsection represent the case where a ranging signal and a command signal are simultaneously present on the uplink carrier. The range clock is taken here to be a sinewave. The ratio of P_C to P_T, the carrier suppression, is

$$\left.\frac{P_C}{P_T}\right|_{\text{U/L}} = J_0{}^2\left(\sqrt{2}\,\phi_r\right) \cdot S_{cmd}(\phi_{cmd}) \qquad (10)$$

The ratio of P_R to P_T is

$$\left.\frac{P_R}{P_T}\right|_{\mathrm{U/L}} = 2J_1{}^2\left(\sqrt{2}\,\phi_r\right) \cdot S_{cmd}(\phi_{cmd}) \tag{11}$$

The ratio of the fundamental command sideband power to P_T is

$$\left.\frac{P_D}{P_T}\right|_{\mathrm{U/L}} = J_0{}^2\left(\sqrt{2}\,\phi_r\right) \cdot M_{cmd}(\phi_{cmd}) \tag{12}$$

where $J_0(\cdot)$ and $J_1(\cdot)$ are Bessel functions of the first kind of order 0 and 1, respectively. These functions are plotted in Figure 4. When the argument x of $J_0(x)$ and $J_1(x)$ is small and positive, the following approximations may be used:

$$J_0(x) \cong 1, \qquad 0 \le x \ll 1 \tag{13}$$

$$J_1(x) \cong x/2, \qquad 0 \le x \ll 1 \tag{14}$$

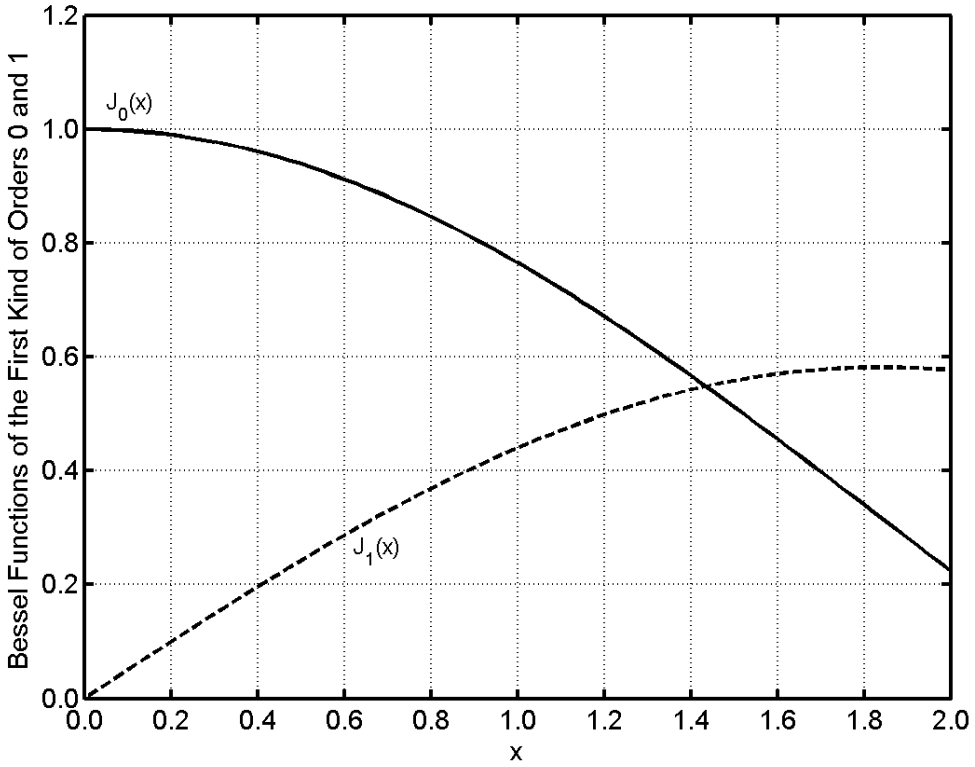

Figure 4. Bessel Functions of the First Kind of Order 0 and 1

The suppression factor $S_{cmd}(\phi_{cmd})$ in Equations (10) and (11) and the modulation factor $M_{cmd}(\phi_{cmd})$ in Equation (12) depend on whether the command signal is bi-polar or uses a sinewave subcarrier. These two factors are given by:

$$S_{cmd}(\phi_{cmd}) = \begin{cases} \cos^2(\phi_{cmd}), & \text{bi-polar} \\ {J_0}^2(\sqrt{2}\,\phi_{cmd}), & \text{sinewave subcarrier} \end{cases} \tag{15}$$

$$M_{cmd}(\phi_{cmd}) = \begin{cases} \sin^2(\phi_{cmd}), & \text{bi-polar} \\ 2{J_1}^2(\sqrt{2}\,\phi_{cmd}), & \text{sinewave subcarrier} \end{cases} \tag{16}$$

In the event that command is absent from the uplink, the factor $S_{cmd}(\phi_{cmd})$ in Equations (10) and (11) can be omitted, since $S_{cmd}(0) = 1$.

2.4.2 Downlink

A turn-around ranging channel demodulates the uplink carrier, filters the baseband signal, applies automatic gain control, and then re-modulates the baseband signal onto the downlink carrier. The AGC serves the important purpose of ensuring that the downlink carrier suppression is approximately constant, independent of received uplink signal level. The bandwidth B_R of the transponder's ranging channel must be larger (typically about 50% larger) than the range-clock frequency, in order to pass the ranging signal with minimal distortion. For example, B_R is typically about 1.5 MHz when the transponder is intended to accommodate a range clock of 1 MHz. Substantial thermal noise from the uplink also passes through this channel. In many deep space scenarios, the thermal noise dominates over the ranging signal in this wideband, turn-around channel. Moreover, command signal from the uplink may pass through this ranging channel. In general, then, noise and command signal as well as the desired ranging signal are modulated onto the downlink carrier whenever the ranging channel is active (Reference 2).

The equations of this subsection represent the case where a ranging signal, a (feedthrough) command signal and noise are simultaneously present in the ranging channel, so that all three of these components, plus telemetry, phase-modulate the downlink carrier. The range clock is taken here to be a sinewave. The ratio of P_C to P_T, the carrier suppression, is

$$\left.\frac{P_C}{P_T}\right|_{\mathrm{D/L}} = {J_0}^2(\sqrt{2}\,\theta_r) \cdot S_{fth}(\theta_{cmd}) \cdot e^{-{\theta_n}^2} \cdot S_{tlm}(\theta_{tlm}) \tag{17}$$

The ratio of P_R to P_T is

$$\left.\frac{P_R}{P_T}\right|_{\mathrm{D/L}} = 2{J_1}^2(\sqrt{2}\,\theta_r) \cdot S_{fth}(\theta_{cmd}) \cdot e^{-{\theta_n}^2} \cdot S_{tlm}(\theta_{tlm}) \tag{18}$$

The ratio of the telemetry sideband power to P_T is

$$\left.\frac{P_D}{P_T}\right|_{\mathrm{D/L}} = {J_0}^2(\sqrt{2}\,\theta_r) \cdot S_{fth}(\theta_{cmd}) \cdot e^{-{\theta_n}^2} \cdot M_{tlm}(\theta_{tlm}) \tag{19}$$

where $J_0(\cdot)$ and $J_1(\cdot)$ are Bessel functions of the first kind of order 0 and 1, respectively.

The command-feedthrough suppression factor $S_{fth}(\theta_{cmd})$ that appears in each of Equations (17), (18) and (19) depends on whether the command signal is bi-polar or uses a sinewave subcarrier. This factor is given by:

$$S_{fth}(\theta_{cmd}) = \begin{cases} \cos^2(\theta_{cmd}), & \text{bi-polar} \\ {J_0}^2\left(\sqrt{2}\,\theta_{cmd}\right), & \text{sinewave subcarrier} \end{cases} \tag{20}$$

In the event that command feedthrough is absent from the ranging channel, the factor $S_{fth}(\theta_{cmd})$ in each of Equations (17), (18) and (19) can be omitted, since $S_{fth}(0) = 1$.

The suppression factor $S_{tlm}(\phi_{tlm})$ in Equations (17) and (18) and the modulation factor $M_{tlm}(\phi_{tlm})$ in Equation (19) depend on whether the telemetry signal is bi-polar or uses a sinewave subcarrier. These two factors are given by:

$$S_{tlm}(\theta_{tlm}) = \begin{cases} \cos^2(\theta_{tlm}), & \text{bi-polar} \\ {J_0}^2\left(\sqrt{2}\,\theta_{tlm}\right), & \text{sinewave subcarrier} \end{cases} \tag{21}$$

$$M_{tlm}(\theta_{tlm}) = \begin{cases} \sin^2(\theta_{tlm}), & \text{bi-polar} \\ 2{J_1}^2\left(\sqrt{2}\,\theta_{tlm}\right), & \text{sinewave subcarrier} \end{cases} \tag{22}$$

For a turn-around ranging channel, the downlink rms phase deviations θ_r, θ_n, and (if command feedthrough is present) θ_{cmd} depend on the ranging signal-to-noise ratio ρ_r and (if command feedthrough is present) the command signal-to-noise ratio ρ_{cmd} in the ranging channel.

$$\rho_r = \left.\frac{P_R}{P_T}\right|_{\mathrm{U/L}} \cdot \left.\frac{P_T}{N_0}\right|_{\mathrm{U/L}} \cdot \frac{1}{B_R} \tag{23}$$

$$\rho_{cmd} = \left.\frac{P_D}{P_T}\right|_{\mathrm{U/L}} \cdot \left.\frac{P_T}{N_0}\right|_{\mathrm{U/L}} \cdot \frac{1}{B_R} \tag{24}$$

where

$P_T/N_0|_{\mathrm{U/L}}$ = uplink total power to noise spectral density ratio, Hz

B_R = noise-equivalent (one-sided) bandwidth of transponder's ranging channel, Hz

In some transponders with a turn-around ranging channel, the AGC is designed to keep constant the average of the absolute value of the voltage at the AGC output. In other transponders, the AGC is designed to keep constant the rms voltage at the AGC output. For both types of AGC, the downlink rms phase deviations θ_r, θ_n, and θ_{cmd} depend on ρ_r and ρ_{cmd} (as well as the parameter θ_{rs}). Turn-around ranging channels with both types of AGC are treated below.

2.4.2.1 AGC with Constant Average of Absolute Value of Voltage

When the transponder's ranging channel has an AGC that keeps constant the average of the absolute value of the channel voltage, there are no exact, analytical expressions for the rms phase deviations θ_r, θ_{cmd} and θ_n. However, these rms phase deviations may be obtained by computer simulation. Curve fits to the simulations appear below.

$$\theta_r = \frac{\theta_{rs}}{1 + \exp[\gamma - 0.79 \cdot \ln(\rho_r)]} \tag{25}$$

where

$$\gamma = \begin{cases} -1.2, & \rho_{cmd} = 0 \\ \ln[0.3 + 0.27 \cdot {\rho_{cmd}}^{0.88}], & \rho_{cmd} > 0 \end{cases} \tag{26}$$

Here $\exp(\cdot)$ and $\ln(\cdot)$ are the exponential function and natural logarithm, respectively. In the event that there is no command feedthrough, $\rho_{cmd} = 0$ and θ_r depends only on the constant parameter θ_{rs} and the ranging signal-to-noise ratio ρ_r. The asymptotes for Equation (25) are $\lim_{\rho_r \to 0} \theta_r = 0$ and $\lim_{\rho_r \to \infty} \theta_r = \theta_{rs}$.

A similar set of equations are valid (approximately) for θ_{cmd}

$$\theta_{cmd} = \frac{\theta_{rs}}{1 + \exp[\chi - 0.79 \cdot \ln(\rho_{cmd})]} \tag{27}$$

where

$$\chi = \ln[0.3 + 0.27 \cdot {\rho_r}^{0.88}] \tag{28}$$

The asymptotes for Equation (27) are $\lim_{\rho_{cmd} \to 0} \theta_{cmd} = 0$ and $\lim_{\rho_{cmd} \to \infty} \theta_{cmd} = \theta_{rs}$.

A curve-fit to the simulation data for θ_n as a function of ρ_r and ρ_{cmd} is:

$$\theta_n = \frac{\theta_{rs} \cdot \left(2/\sqrt{\pi}\right)}{1 + \exp[-0.87 + 0.81 \cdot \ln(\rho_{rss})]} \tag{29}$$

where ρ_{rss} is the root-sum-square of ρ_r and ρ_{cmd}:

$$\rho_{rss} = \sqrt{{\rho_r}^2 + {\rho_{cmd}}^2} \tag{30}$$

The asymptotes for this curve are $\lim_{\rho_{rss} \to 0} \theta_n = \theta_{rs} \cdot \left(2/\sqrt{\pi}\right)$ and $\lim_{\rho_{rss} \to \infty} \theta_n = 0$.

Since θ_r is directly proportional to the parameter θ_{rs}, the ratio θ_r/θ_{rs} may be plotted as a function of ρ_r (and ρ_r alone when $\rho_{cmd} = 0$). This appears in Figure 5 for the case of no command feedthrough: $\rho_{cmd} = 0$ and $\theta_{cmd} = 0$. The solid curve labeled AAV is valid for a turn-around ranging channel whose AGC keeps constant the average of the absolute voltage (AAV). Figure 5 shows that the ratio θ_r/θ_{rs} increases monotonically as a function of ρ_r with a limiting value of 1. (In other words, the strong-signal value of θ_r is θ_{rs}.) The AAV curve of Figure 5 comes from Equations (25) and (26) with $\rho_{cmd} = 0$.

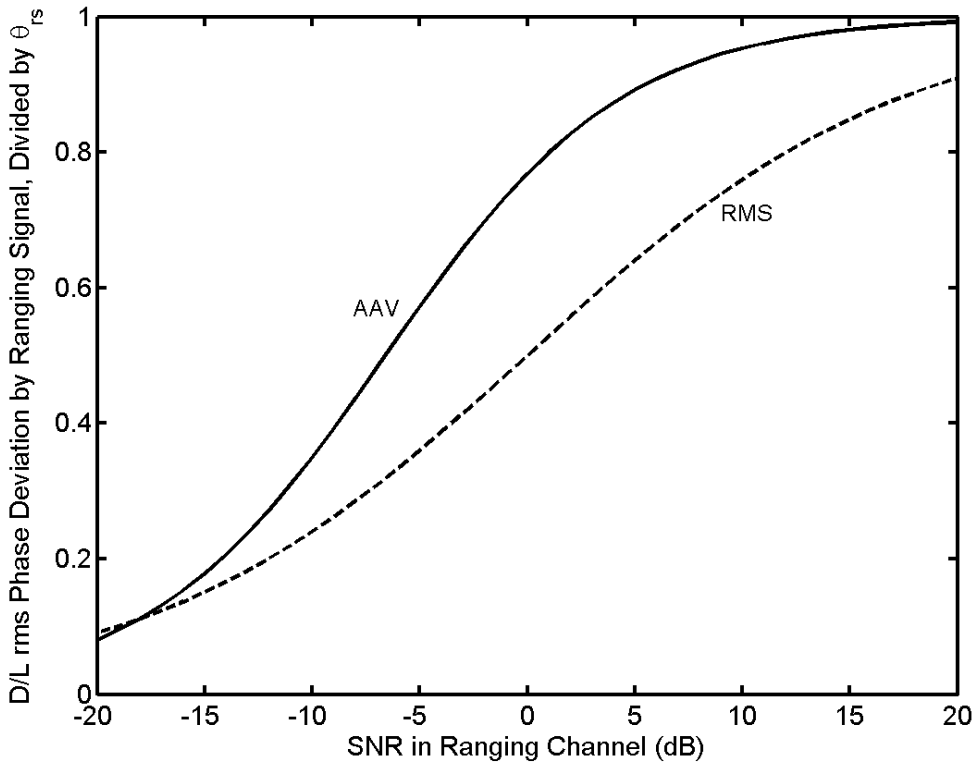

Figure 5. Downlink rms Phase Deviation by Ranging Signal (No Command Feedthrough)

The ratio θ_n/θ_{rs} may also be plotted as a function of ρ_r when $\rho_{cmd} = 0$. This appears in Figure 6. The solid curve labeled AAV is valid for a turn-around ranging channel whose AGC keeps constant the average of the absolute voltage (AAV). Figure 6 shows that the ratio θ_n/θ_{rs} decreases monotonically as a function of ρ_r. The AAV curve of Figure 6 comes from Equations (29) and (30) with $\rho_{cmd} = 0$.

2.4.2.2 AGC with Constant Root-Mean-Square Voltage

In some transponders, especially older designs, the ranging channel has an AGC that enforces a constant rms voltage at the AGC output. Since an unchanging rms voltage corresponds to an unchanging power, this type of AGC is also called a power-controlled AGC.

An AGC that enforces constant rms voltage (equivalently, constant power) at the AGC output is characterized by the following relationship among the rms phase deviations θ_r, θ_{cmd}, θ_n, and θ_{rs}.

$$\theta_r{}^2 + \theta_{cmd}{}^2 + \theta_n{}^2 = \theta_{rs}{}^2 \tag{31}$$

In other words, the total power in the turn-around ranging channel, which equals the ranging signal power plus the feedthrough command signal power plus the noise power in the channel bandwidth, equals a constant value. The rms phase deviations are given by

$$\theta_r = \theta_{rs} \cdot \sqrt{\frac{\rho_r}{1 + \rho_r + \rho_{cmd}}} \tag{32}$$

$$\theta_{cmd} = \theta_{rs} \cdot \sqrt{\frac{\rho_{cmd}}{1 + \rho_r + \rho_{cmd}}} \tag{33}$$

$$\theta_n = \frac{\theta_{rs}}{\sqrt{1 + \rho_r + \rho_{cmd}}} \tag{34}$$

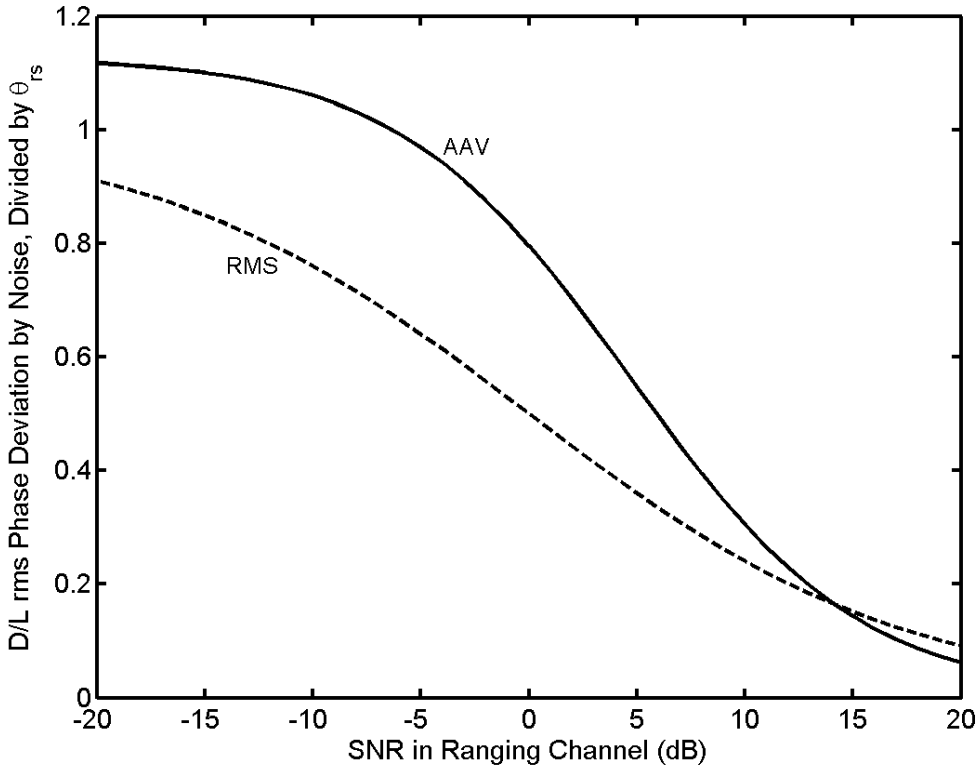

Figure 6. Downlink rms Phase Deviation by Noise (No Command Feedthrough)

The ratio θ_r/θ_{rs} is plotted as a function of ρ_r in Figure 5 for the case of no command feedthrough: $\rho_{cmd} = 0$ and $\theta_{cmd} = 0$. The dashed curve labeled RMS is valid for a turn-around ranging channel whose AGC enforces a constant rms voltage at the AGC output. The RMS curve of Figure 5 comes from Equation (32) with $\rho_{cmd} = 0$.

The ratio θ_n/θ_{rs} is plotted as a function of ρ_r in Figure 6 for the case of no command feedthrough: $\rho_{cmd} = 0$ and $\theta_{cmd} = 0$. The dashed curve labeled RMS is valid for a turn-around ranging channel whose AGC enforces a constant rms voltage at the AGC output. The RMS curve of Figure 6 comes from Equation (34) with $\rho_{cmd} = 0$.

2.4.2.3 Comparison of Two AGC Types

As explained above, there are two types of AGC that have been employed in transponders with turn-around ranging channels. These two AGCs differ in the quantity that is kept constant: either the average of the absolute voltage (AAV) or the root-mean-square (RMS).

Figure 7 plots $P_R/P_T|_{D/L}$ as a function of ρ_r for each of the two AGC types. For all curves in this figure, there is no telemetry and there is no command feedthrough. For each AGC type, there are two curves: one for $\theta_{rs} = 0.2$ rad rms and a second for $\theta_{rs} = 0.4$ rad rms. $P_R/P_T|_{D/L}$ was calculated using Equation (18). The phase deviations θ_r and θ_n needed within Equation (18) were calculated using the equations of Subsection 2.4.2.1 for the AAV curves and Subsection 2.4.2.2 for the RMS curves.

Figure 8 plots the carrier suppression $P_C/P_T|_{D/L}$ as a function of ρ_r for each of the two AGC types. For all curves in this figure, there is no telemetry and there is no command feedthrough. For each AGC type, there are two curves: one for $\theta_{rs} = 0.2$ rad rms and a second for $\theta_{rs} = 0.4$ rad rms. $P_C/P_T|_{D/L}$ was calculated using Equation (17). The phase deviations θ_r and θ_n needed within Equation (17) were calculated using the equations of Subsection 2.4.2.1 for the AAV curves and Subsection 2.4.2.2 for the RMS curves.

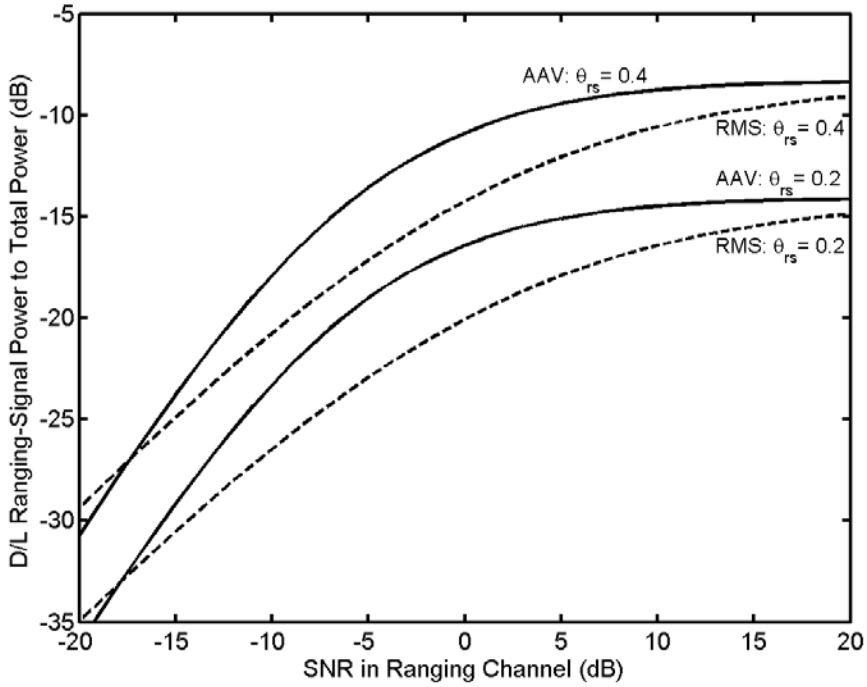

Figure 7. Downlink Ranging-Signal Power to Total Power (No Telemetry, No Command)

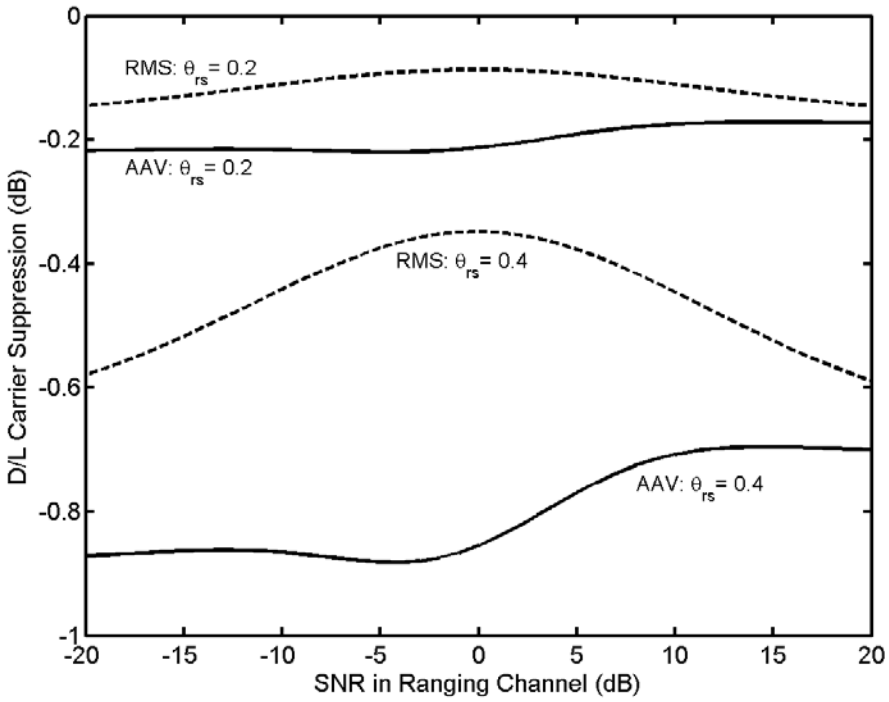

Figure 8. Downlink Carrier Suppression (No Telemetry, No Command)

2.5 Uplink Spectrum

The spectrum of the uplink carrier is of some concern because of the very large transmitter power used on the uplink for deep space missions. In the interest of spectral efficiency, the ranging signal is filtered prior to passing to the phase modulator for the uplink carrier. This is accomplished with the uplink ranging filter, which is digitally implemented within the USG. The uplink ranging filter is a low-pass filter with a configurable bandwidth. The default (and minimum) bandwidth is 1.2 MHz.

Below are some examples of the spectrum of an uplink carrier when ranging is present. It is assumed that ranging is the only signal that modulates the uplink carrier in all examples given here. In the more general case, where command and ranging are both present, the spectrum would be similar to that indicated below except that the ranging sidebands would be reduced by an extra suppression factor due to the presence of command and there would also be command sidebands and intermodulation products. In general, the calculation of the spectrum is quite complicated.

Since the ranging sequence consists of a set of periodic signals, the spectrum for every ranging component consists of a set of discrete spectral lines. The ratio of the power in any one discrete spectral line to the total uplink power is denoted here

$$\frac{P_k}{P_T} = \left\{ \begin{array}{c} \text{fraction of uplink total power} \\ \text{in the discrete spectral line} \\ \text{with frequency } f_C + kf_R \end{array} \right. \tag{35}$$

where f_C is the uplink carrier frequency, k is an integer harmonic number, and f_R is the frequency of the range component that presently modulates the carrier. The spectrum is symmetric about the carrier: for every discrete spectral line at $f_C + kf_R$ there is another of equal power at $f_C - kf_R$. When ranging alone modulates the carrier, the ratios of Equation (35) are subject to the conservation-of-energy law:

$$\frac{P_0}{P_T} + 2\sum_{k=1}^{\infty}\frac{P_k}{P_T} = 1 \tag{36}$$

The first term in Equation (36), P_0/P_T, represents the ratio of the residual-carrier power to the total power P_T.

When the range component is a sinewave (such as the range clock, for example, when the third and higher-order harmonics have been blocked by the uplink ranging filter), the relative powers of the discrete spectral lines are given by

$$\frac{P_k}{P_T} = {J_k}^2\left(\sqrt{2}\,\phi_r\right) \tag{37}$$

ϕ_r is the rms phase deviation of the uplink carrier by the ranging signal. $J_k(\cdot)$ is the Bessel function of the first kind of order k. The spectrum defined by Equation (37) is illustrated in Figure 9 for the case of a range-clock frequency $f_{RC} = 1$ MHz and $\phi_r = 0.80$ rad rms, corresponding to 3 dB of carrier suppression.

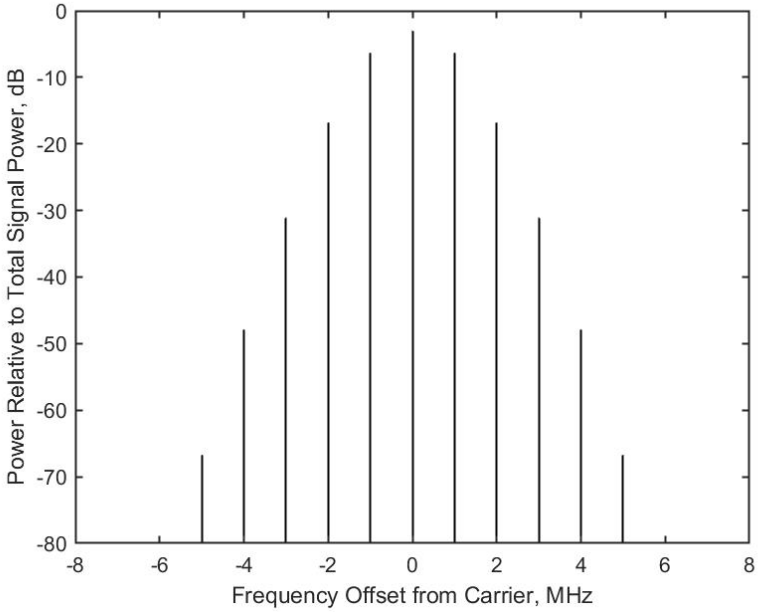

Figure 9. Spectrum: Sinewave Range Clock
$f_{RC} = 1$ MHz, $\phi_r = 0.80$ rad rms

During those periods when an ambiguity-resolving component is multiplied by a chop component, the spectrum of the uplink carrier consists of discrete spectral lines, as indicated in Equation (35). Figure 10 shows the spectrum of a 125-kHz component chopped by the range clock. In this example, $\phi_r = 0.80$ rad rms and the chop component, which is the range clock, is a sinewave and has a frequency $f_{RC} = 1$ MHz. The effect of the uplink ranging filter has been taken into account in Figure 10. The uplink spectrum would be much broader in the absence of the uplink ranging filter; the spectrum without filtering is shown in Figure 11.

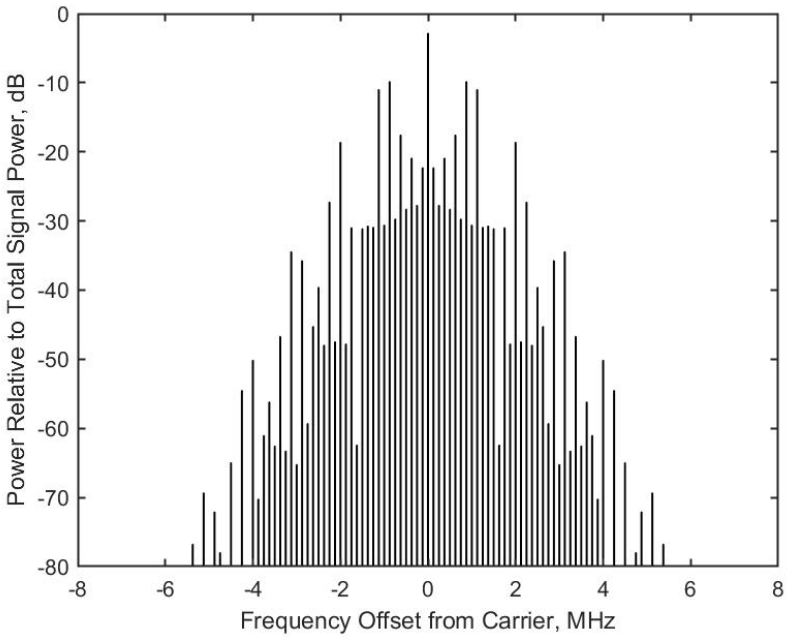

Figure 10. Spectrum: 125-kHz Component Chopped by Range Clock
$f_{RC} = 1$ MHz, $\phi_r = 0.80$ rad rms

2.6 Range Measurement Performance

Thermal noise has two effects on range measurements. First, there is a standard deviation of range measurement error due to thermal noise. Second, there is a probability of acquisition of the range measurement that is less than 100% due to the presence of thermal noise.

2.6.1 Range Measurement Error Due to Thermal Noise

The standard deviation σ_ρ of range measurement error, in meters rms, due to downlink thermal noise is given by

$$\sigma_\rho = \frac{c}{f_{RC} \cdot \sqrt{32\pi^2 \cdot T_1 \cdot (P_R/N_0)}} \tag{38}$$

where

c = speed of electromagnetic waves in vacuum, $299{,}792{,}458$ m/s

T_1 = integration time for range clock, s

f_{RC} = frequency of the range clock, Hz

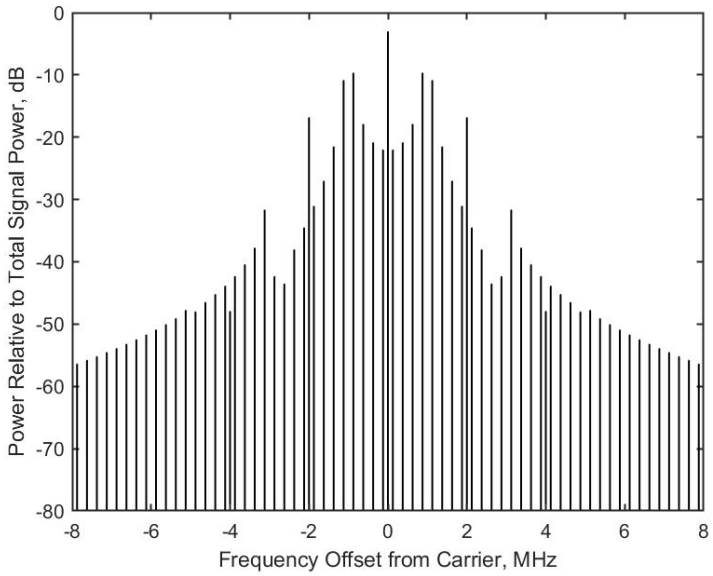

Figure 11. Unfiltered Spectrum: 125-kHz Component Chopped by Range Clock
$f_{RC} = 1$ MHz, $\phi_r = 0.80$ rad rms

Equation (38) is valid for the case of a sinewave range clock and a matching sinewave local model of the range clock at the RRT.

P_R/N_0, the ratio of the downlink ranging signal power to the noise spectral density, is given by

$$\frac{P_R}{N_0} = \frac{P_R}{P_T}\bigg|_{\mathrm{D/L}} \cdot \frac{P_T}{N_0}\bigg|_{\mathrm{D/L}} \tag{39}$$

where $P_T/N_0|_{\mathrm{D/L}}$ is the downlink total signal to noise spectral density ratio and where $P_R/P_T|_{\mathrm{D/L}}$ is the ratio of downlink ranging signal power to total power, which is given in Equation (18).

P_R is reduced by the effect of uplink noise and any command feedthrough. This can be understood by noting that $P_R/P_T|_{\mathrm{D/L}}$, as given in Equation (18), depends on the rms phase deviations θ_r, θ_{cmd}, and θ_n; and these rms phase deviations depend, in turn, on the ranging signal-to-noise ratio ρ_r in the transponder's ranging channel.

The standard deviation of range measurement error (m) due to thermal noise is plotted in Figure 12 against the product $T_1 \cdot (P_R/N_0)$, expressed in decibels: $10\log(T_1 \cdot P_R/N_0)$. These curves were calculated from Equation (38) for three different values of range-clock frequency: 250 kHz, 500 kHz, and 1 MHz.

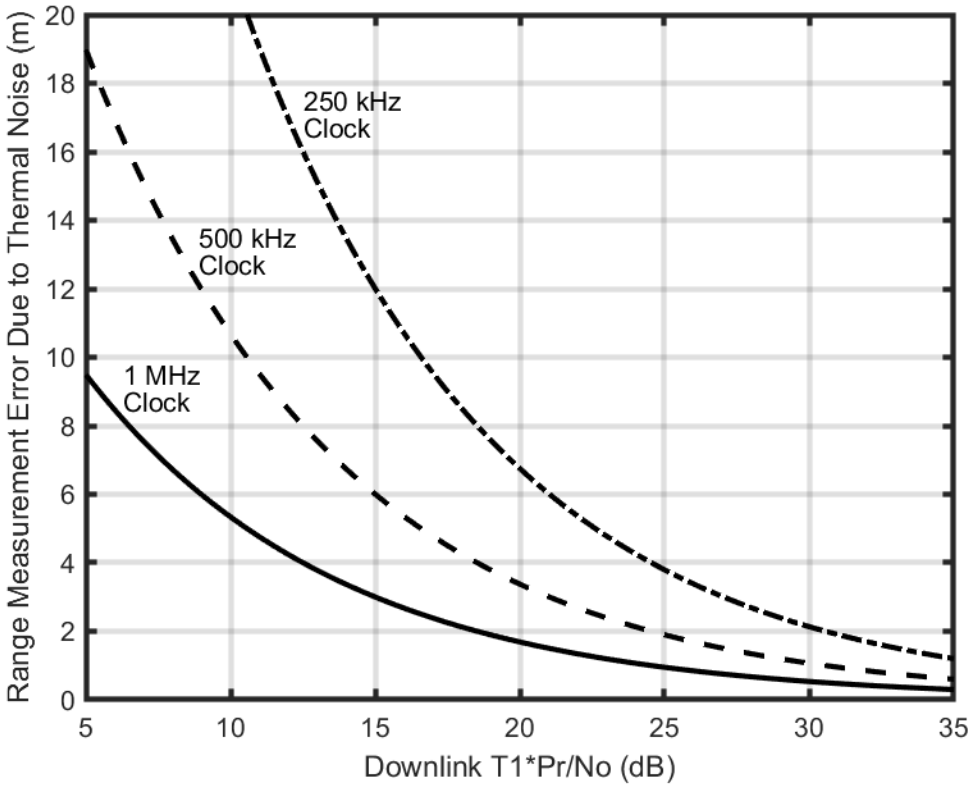

Figure 12. Range Measurement Error for Sinewave Range Clock

When σ_ρ has a specified value and an estimate is available for P_R/N_0, the required integration time T_1 can be found by a rewriting of Equation (38):

$$T_1 = \frac{c^2}{32\pi^2 \cdot {f_{RC}}^2 \cdot (P_R/N_0) \cdot {\sigma_\rho}^2} \tag{40}$$

The standard deviation of the two-way time delay σ_τ, in seconds, is related to σ_ρ, as given in Eq. (38), by

$$\sigma_\tau = \frac{2}{c} \cdot \sigma_\rho \tag{41}$$

The factor of 2 in Eq. (41) accounts for the fact that σ_ρ characterizes the error in the *one*-way range, while σ_τ characterizes the error in a *two*-way time delay. The standard deviation of the two-way phase delay σ_{RU}, as measured in range units, is related to σ_τ by

$$\sigma_{RU} = \begin{cases} \dfrac{f_S}{2} \cdot \sigma_\tau, & \text{S-band uplink} \\ \dfrac{221}{749} \cdot \dfrac{f_X}{2} \cdot \sigma_\tau, & \text{X-band uplink} \\ \dfrac{221}{3599} \cdot \dfrac{f_{Ka}}{2} \cdot \sigma_\tau, & \text{Ka-band uplink} \end{cases} \tag{42}$$

where f_S is the frequency of an S-band uplink carrier, f_X is the frequency of an X-band uplink carrier, and f_{Ka} is the frequency of a Ka-band uplink carrier.

2.6.2 Probability of Acquisition

A correct determination of the range can only happen if the ambiguity is correctly resolved. This is accomplished with a set of correlations within the RRT between the received baseband ranging signal and local models of the ambiguity-resolving components. A range measurement is successfully acquired when every ambiguity-resolving correlation is correctly determined. The probability of acquisition P_{acq} for the range measurement is

$$P_{\text{acq}} = \left[\frac{1}{2} + \frac{1}{2}\,\text{erf}\left(\sqrt{T_2 \cdot P_R/N_0}\right)\right]^{N_C} \tag{43}$$

where T_2 is the integration time for each ambiguity-resolving component and N_C is the number of ambiguity-resolving components in the ranging sequence,

$$N_C = n_L - n_{RC} \tag{44}$$

This is the difference between the component number n_L of the last (smallest-frequency) component and the component number n_{RC} of the range clock. For example, if the range clock is component 4 (approximately 1 MHz) and the last component is 20, then $N_C = 16$. (In this case, the ranging sequence consists of the range clock followed by 16 ambiguity-resolving components.) The error function erf(·) is defined by

$$\text{erf}(y) = \frac{2}{\sqrt{\pi}} \int_0^y e^{-t^2}\, dt \tag{45}$$

The value that Equation (43) gives for P_{acq} is, in general, greater than 0 and less than 1. P_{acq} is often characterized as a percentage (between 0% and 100%).

P_{acq} is plotted in Figure 13 as a function of the product $T_2 \cdot (P_R/N_0)$, in decibels: $10 \log(T_2 \cdot P_R/N_0)$. The functional dependence is shown for three representative values of N_C: 10, 15, and 20. The curves in this figure were calculated from Equation (43).

It will often be necessary to work the problem in the reverse direction. For a specified P_{acq}, what is the required value for $T_2 \cdot P_R/N_0$? Of course, this question can be answered approximately by applying a graphical method to Figure 13. Table 3 provides a more accurate method; this table lists required values for $T_2 \cdot P_R/N_0$ (in decibels) as a function of $\log(P_{\text{acq}})/N_C$. Here $\log(\cdot)$ is is the common logarithm (the base-10 logarithm). This table is based on Equation (43).

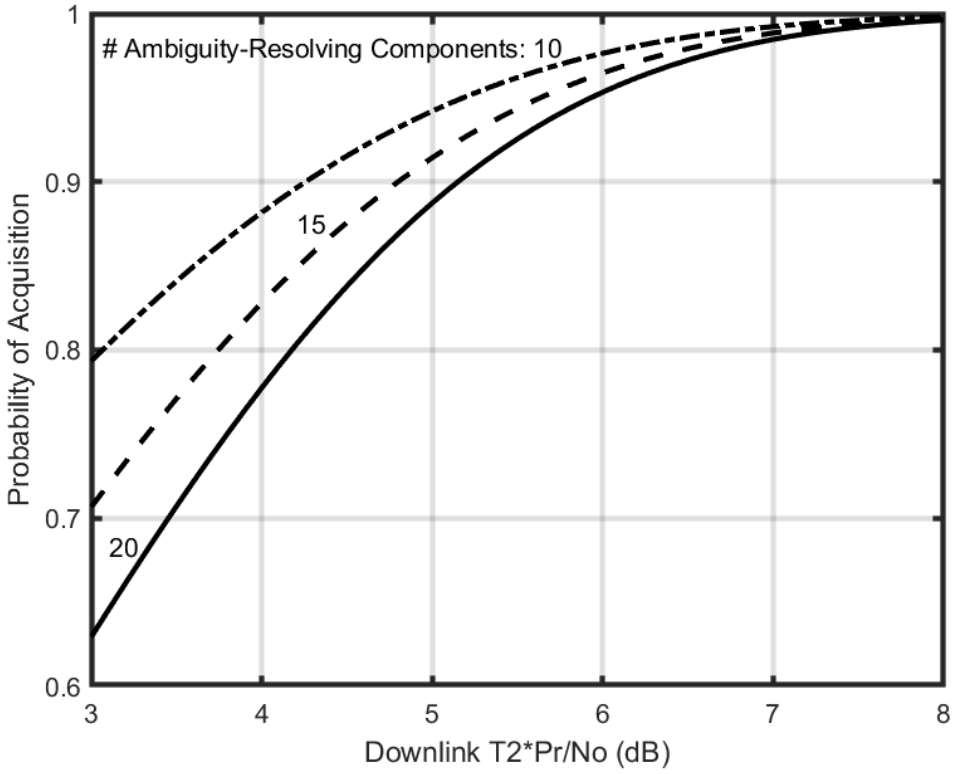

Figure 13. Probability of Acquisition

Here is an example of how Table 3 can be used. If the desired P_{acq} is 0.95 and N_C is 16, then $\log(P_{\text{acq}})/N_C = -0.00139$. From Table 3, the decibel values 5.3 dB and 6.1 dB are found for $\log(P_{\text{acq}})/N_C = -0.0020$ and $\log(P_{\text{acq}})/N_C = -0.0010$, respectively. An interpolation suggests that $T_2 \cdot P_R/N_0$ must be about 5.8 dB in order to acquire correctly with $P_{\text{acq}} = 0.95$ when $N_C = 16$.

In a computational environment where a special function like erf(·) is not available, it is useful to have an algebraic approximation to Equation (43). Here is such an approximation:

$$P_{\text{acq}} = \begin{cases} [c_3 Z^3 + c_2 Z^2 + c_1 Z + c_0]^{N_C}, & 0 \le Z \le 8.0 \\ 1.00, & Z > 8.0 \end{cases} \tag{46}$$

where Z is the product $T_2 \cdot (P_R/N_0)$ in units of decibels,

$$Z = 10 \log[T_2 \cdot (P_R/N_0)] \quad \text{dB} \tag{47}$$

The coefficients for the model of Equation (46) are given in Table 4. The Equation (46) model is not reliable for $Z < 0$ dB. For $Z > 8.0$ dB, it is approximately true that $P_{\text{acq}} = 1$.

Table 3. Interpolation Table
Required $T_2 \cdot P_R/N_0$ (in decibels) for Given $\log(P_{\text{acq}})/N_C$

$\frac{\log(P_{\text{acq}})}{N_C}$	$T_2 \cdot (P_R/N_0)$ dB
-0.0300	0.7
-0.0200	1.6
-0.0100	3.0
-0.0080	3.4
-0.0060	3.9
-0.0040	4.5
-0.0030	4.8
-0.0020	5.3
-0.0010	6.1
-0.0008	6.3
-0.0006	6.6
-0.0004	7.0
-0.0003	7.4
-0.0002	8.0

Table 4. Coefficients for Equation (46)

c_3	0.000158
c_2	-0.003843
c_1	0.031437
c_0	0.9131

The recommended range for P_R/N_0 is -20 dB-Hz to $+50$ dB-Hz. Range measurement performance has been validated down to -20 dB-Hz. At this low end of performance, however, the integration times are quite large. (For a given measurement accuracy,

the smaller P_R/N_0, the larger must be the integration times.) Although there is no upper limit on P_R/N_0, a value in excess of $+50$ dB-Hz is not needed. Moreover, two downlink estimators—that for the symbol signal-to-noise ratio and that for the system noise temperature—become inaccurate when P_R/N_0 is large (see Subsection 2.6.6).

2.6.3 Selection of Integration Times

Thermal noise sets lower limits on the integration times T_1 and T_2. For a specified σ_ρ, a given f_{RC} and an estimated available P_R/N_0, a minimum required integration time T_1 may be calculated from Equation (40). For a specified P_{acq}, a N_C dictated by considerations of ambiguity resolution, and an estimated available P_R/N_0, a minimum required integration time T_2 may be found with the aid of Table 3.

If the RTLT changes by more than about 1 second during a tracking pass in which ranging is done, then the integration times T_1 and T_2 should be increased beyond the values calculated from thermal-noise considerations. Subsection 2.6.5.2 offers guidance in this matter.

2.6.4 Three-Way Ranging

Three-way ranging may be done if the RTLT is too large for two-way ranging. One station transmits a ranging sequence to the spacecraft where it is received and re-transmitted. A second station receives the ranging sequence and performs the necessary correlations.

Three-way ranging yields less accurate results than two-way ranging. There are two reasons for this. First, the station delays cannot be accurately calibrated for three-way ranging. Second, the clock offset between the transmitter and receiver is imperfectly known.

Ideally, in order to get the best three-way ranging measurements, the transmitting station's one-way uplink delay and the receiving station's one-way downlink delay should be removed from the measured three-way delay. However, these one-way delays cannot be measured directly. Instead, the two-way station delay of each station is measured with the assumption that half of the delay is in the uplink equipment and the other half is in the downlink equipment. The two round-trip station delays are averaged, and this average is subtracted from the round-trip phase delay to the spacecraft. This average is only as accurate as the approximation that the delay is equally distributed between the uplink and downlink at both stations.

Three-way range measurement error is often dominated by a clock offset between the time reference at the transmitting and receiving stations. This clock offset can be as large as 9 μs (3σ), and there is an additional small uncertainty in the delay between the station clock and the exciter or receiver (see Module 304). The largest part of the clock offset can be determined and removed from the range measurement. However, the remaining (unmodeled) clock offset translates directly into an error in the three-way range measurement.

2.6.5 Ranging Anomalies Related to Sequence Timing

It has been observed that there can be problems with range measurements when the integration time T_2 is very short or when the RTLT changes during a single tracking pass by an amount comparable with T_2. These anomalies, along with suggested remedies, are discussed below.

2.6.5.1 Short Integration Time T_2

If a very short integration time such as 1 or 2 s is used for T_2, the effective integration time of each ambiguity-resolving component may be significantly less that the design value of T_2. This happens if the downlink integration interval for each ambiguity-resolving component does not completely overlap the received component being integrated (as discussed in Section 2.2). The difference between the design T_2 and the effective integration time will typically be a fraction of a second.

The user may suspect this problem when a very small T_2 is being used and the number of range blunder points is more than the Probability of Acquisition Tolerance should permit. The simplest solution is to increase the design T_2. It will often suffice to increase T_2 by just 1 s.

2.6.5.2 Changing RTLT

The effective integration time of each component (the range clock as well as the ambiguity-resolving components) is reduced for some range measurements if the RTLT varies significantly during a tracking pass. The estimated RTLT that is applied to ranging operations for a tracking pass is typically correct at the beginning of the pass. But if the actual RTLT moves away from this estimated value by a few seconds during the pass, a misalignment arises for range measurements occurring later in the pass. This causes the integration of any given component of measurements made later in the pass to slip so that there is not a complete overlap with the received component. The result can be an increase in the range measurement error and a decrease in the probability of range acquisition.

The preferred solution to the problem of a changing RTLT is to use larger values for the integration times, with due consideration for the variability of the RTLT. With this solution, the range measurements will not degrade significantly as the tracking pass proceeds. In the description of this solution, ΔRTLT represents the absolute value of the change in RTLT over the course of a ranging pass.

If ΔRTLT exceeds 1 s, the integration time T_1 should be increased by $\lceil \Delta\text{RTLT} - 1 \rceil$, where $\lceil \cdot \rceil$ is the ceiling function (the smallest integer that is greater than or equal to its argument). Two examples are given here. If $1 \text{ s} < \Delta\text{RTLT} \leq 2 \text{ s}$, T_1 should be increased by 1 s. If $2 \text{ s} < \Delta\text{RTLT} \leq 3 \text{ s}$, T_1 should be increased by 2 s.

If ΔRTLT exceeds 0.5 s, the integration time T_2 should be increased by $\text{round}(\Delta\text{RTLT})$, where $\text{round}(\cdot)$ indicates rounding to the nearest integer. Two examples are given here. If $0.5 \text{ s} < \Delta\text{RTLT} \leq 1.5 \text{ s}$, T_2 should be increased by 1 s. If $1.5 \text{ s} < \Delta\text{RTLT} \leq 2.5 \text{ s}$, T_2 should be increased by 2 s.

An alternative solution is to stop the downlink range measurements whenever the difference between the estimated RTLT and the actual RTLT exceeds some threshold and restart the downlink range measurements with an updated RTLT estimate. In order to maintain the quality of the range measurements while using the smallest possible integration times, it may be necessary to stop and restart the downlink range measurements multiple times during some tracking passes. This will be particularly true for missions having a fast-changing RTLT and small integration times. The first solution, discussed in the previous paragraph, will ordinarily be the preferred solution, due to its simplicity.

P_R/N_0, the ratio of the downlink ranging signal power to the noise spectral density, is estimated by the RRP during range measurements, and the estimate is included in the delivered data. An accurate estimate depends on having a value for RTLT that is correct to within about 1 s. When the RTLT changes, during a tracking pass, by more than about 1 s, P_R/N_0 is underestimated during the later part of the tracking pass. This effect is most noticeable for large values of P_R/N_0.

2.6.6 Interference Caused by Sequential Ranging

Sequential ranging has, on occasion, been a source of interference to conical-scan tracking and to the downlink signal power estimators. This interference is usually only an issue during early mission phase when signal-to-noise ratios are very high.

Perhaps the best-known case of such interference occurred with the Ulysses spacecraft. In that case, sequential ranging caused variations in the uplink carrier suppression, which was a problem for the conical-scan (conscan) pointing of the high-gain antenna on the Ulysses spacecraft. This is not a general problem because conscan is not used for pointing most spacecraft antennas. Furthermore, this problem for Ulysses occurred at a time when a squarewave was being used for the 1-MHz range clock. At present, a 1-MHz range clock is filtered and approximates a sinewave, and with a sinewave range clock the variation in carrier suppression is much reduced.

Sequential ranging has also, on occasion, caused variations in the downlink residual-carrier power, which can interfere with the conscan pointing of the DSS antenna (Reference 2). This only happens when the ranging signal-to-noise ratio is large, as occurs sometimes during the early phase of a mission.

It has been observed in the early phase of some missions, shortly after launch when the signal-to-noise ratios are large, that sequential ranging can cause variations in some of the downlink signal power estimators. In particular, the symbol signal-to-noise ratio estimate may be low when a strong ranging signal is present on the downlink. This is due to the fact that the ranging signal looks like noise to the estimator. The symbol signal-to-noise ratio estimate is used as an input by the algorithm that estimates the system noise temperature. When the symbol signal-to-noise ratio estimate is low, the system noise temperature estimate is high. Both estimates have been observed to be affected by the presence of a strong ranging signal.

2.7 Range Corrections

Range is defined to be the distance from the reference point on the DSS antenna to the reference point on the spacecraft antenna. The reference point of a DSS antenna is the intersection of the azimuth and elevation axes. When the two-way time delay is measured, the result includes more than just the two-way delay between the reference points of the DSS and spacecraft antennas. The measured two-way delay also includes station delay and spacecraft delay. These extra delays must be determined through calibration and then removed from the measured two-way time delay. The spacecraft delay is measured during DSN compatibility testing prior to launch. The station delay is determined in two parts: the DSS delay and the Z-correction.

A range measurement (that has not yet been corrected) provides the two-way delay through the station uplink path, starting from the USG, to and from the spacecraft, and through the station downlink path, ending in the RRT. Figure 14 illustrates the two-way signal path at the station. It is necessary to determine the uplink station delay for the path from the USG to the antenna reference point, to determine the downlink station delay for the path from the antenna reference point to the RRT, and to remove these delays from the measured two-way delay.

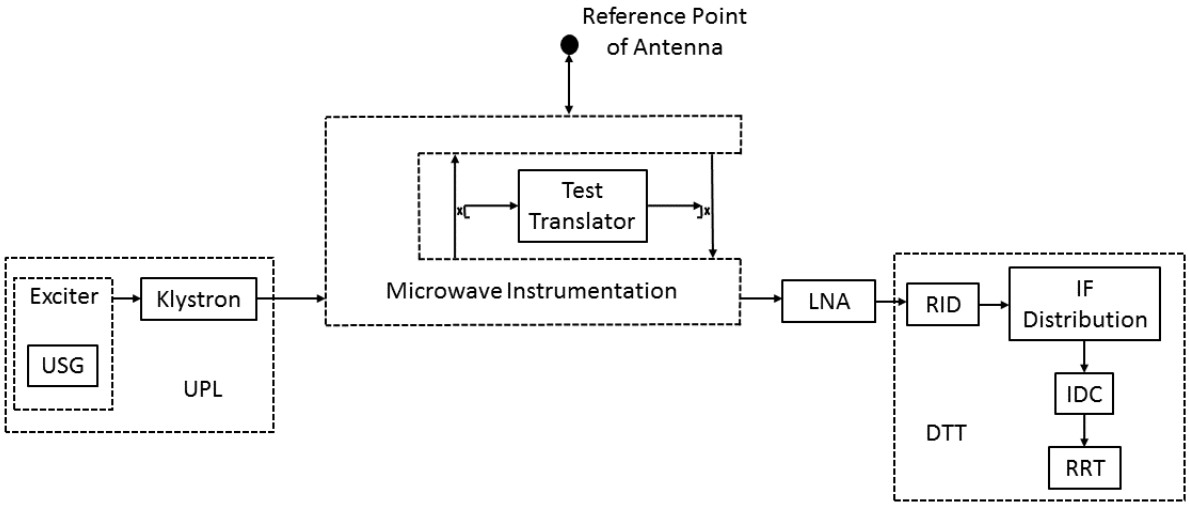

Figure 14. DSS Delay Calibration

2.7.1 DSS Delay

The DSS delay is obtained by a calibration that mimics an actual two-way range measurement, except that the signal path lies entirely within the station. A portion of the uplink carrier is diverted through a coupler to a test translator. The test translator shifts the carrier to the downlink frequency (while not altering the modulation) and feeds this frequency-shifted carrier to a coupler that places it on the downlink path within the station. The DSS delay contains most of the station delay. To be precise, the DSS delay comprises the delay from the USG to the ranging coupler on the uplink, the delay through the test translator (and its cables), and the delay from the ranging coupler on the downlink to the RRT.

Figure 14 is a somewhat abstract representation of the configuration. The microwave instrumentation shown in this figure is not an official subsystem, rather it is a conceptual grouping of microwave signal paths and microwave devices. On the uplink, the uplink carrier that is output from the klystron passes through the microwave instrumentation on its way to the reference point of the antenna. On the downlink, the downlink passes through the microwave instrumentation on its way to the LNA. Along the uplink path, a portion of the uplink carrier is coupled to the test translator. The portion of the carrier that has been frequency shifted to the downlink band inside the test translator is then coupled to the downlink path. The specific details of the microwave instrumentation are generally different at different DSSs and for different bands within a given DSS. Modules 101, 103 and 104 should be consulted for those details.

The DSS delay is station and configuration dependent. It should be measured for every ranging pass. This measurement is called precal for pre-track calibration and postcal for post-track calibration. The former is done at the beginning of a ranging pass; the latter is only needed when there is a change in equipment configuration during the track or precal was not performed due to a lack of time.

The DSS delay varies significantly as a function of carrier frequency. This is illustrated in Figure 15 for an X-band (uplink and downlink) calibration at DSS 63. The vertical axis on this plot is the DSS delay, labeled STDL in this plot. The difference between the largest and smallest delays over the 8400—8450 MHz band is about 18 ns in this case. On both the lower and upper ends of this band, the rise in station delay originates in the klystron on the uplink side of the station. The ripple in the station delay arises from impedance mismatches; every transmission line that has some mismatch at both ends will introduce ripple in the group delay.

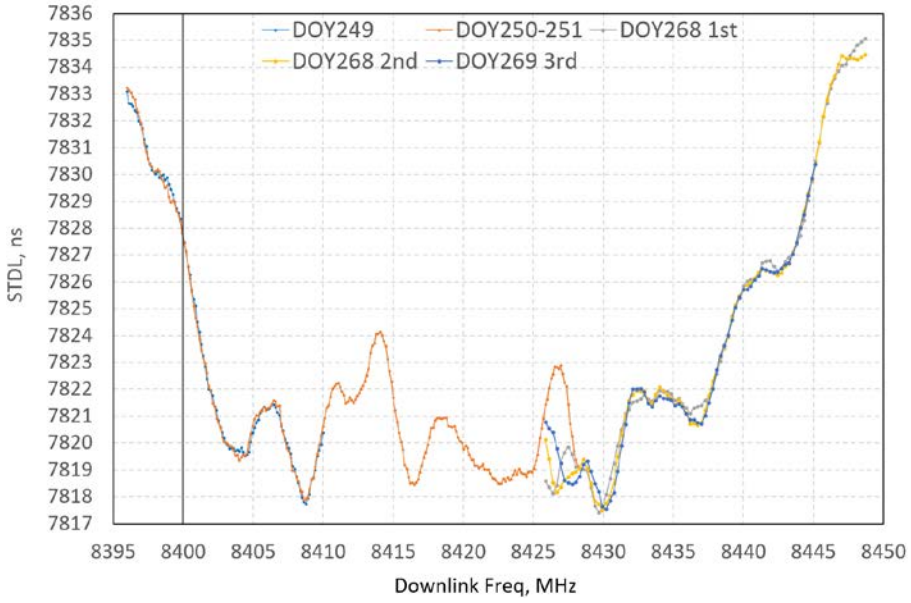

Figure 15. DSS Delay as a Function of Downlink Frequency

2.7.2 Z-Correction

The DSS delay itself must be corrected. This is accomplished with the Z-correction. The DSS delay includes the delay through the test translator (and its cables), but the test translator is not in the signal path of an actual range measurement. Moreover, the DSS delay does not include, but should include, the delays between the ranging couplers and the antenna reference point.

The Z-correction is defined as the delay through the test translator (and its cables) minus the uplink and downlink delays between the ranging couplers and the antenna reference point. The DSS delay minus the Z-correction therefore gives the delay between the USG and the antenna reference point plus the delay between the antenna reference point and the RRT. This is

exactly the quantity that must be subtracted from a range measurement in order to produce a two-way delay relative to the antenna reference point.

The test translator delay is measured by installing a zero delay device (ZDD) in place of the test translator. Since the ZDD delay is measured in the laboratory, the signal delay contributed by the test translator can be calculated to a known precision. This measurement is made approximately once each year or when there are hardware changes in this portion of the signal path. The delays between the ranging couplers and the antenna reference point are stable and need not be updated often; they are determined by a combination of calculation and measurement.

2.8 Total Error for Range Measurement

Several error sources contribute to the total error for a range measurement. For two-way range measurement, the two most important error sources are typically thermal noise and station calibration error. The error due to thermal noise is discussed in Section 2.6. The error in calibrating and removing the station delay is often the dominant error source for two-way ranging. For two-way range measurements in the X band, there is typically about 6 ns of station calibration error in the two-way delay, corresponding to a (one-way) range error of about 1 meter.

The error in calibrating and removing the spacecraft delay is stable for a given spacecraft and a given band pairing (for example, X band on the uplink and X band on the downlink). The orbit determination program can, given enough range measurements for this spacecraft and band pairing, solve for this error.

There are error contributions, usually small compared to the station calibration error, due to the passage of the uplink and downlink through the troposphere, ionosphere and solar corona (Reference 3). When the angle between the sun and the spacecraft, as seen from the station, is small and the spacecraft is beyond the sun, the error contribution from the solar corona can become the dominant contributor to error in the range measurement.

For three-way ranging (in which one station transmits the uplink and a second station receives the downlink), the total delay measurement error is larger than for two-way. There are two reasons for this. First, there is a clock offset between the transmitting and receiving stations. Second, the calibration of the station delays is more difficult to achieve accurately in this case.

Appendix: Glossary of Parameters

$P_T/N_0\|_{\mathrm{U/L}}$	ratio of uplink total power to noise spectral density, Hz
$P_C/P_T\|_{\mathrm{U/L}}$	ratio of uplink residual-carrier to total power
$P_R/P_T\|_{\mathrm{U/L}}$	ratio of uplink ranging-signal to total power
$P_D/P_T\|_{\mathrm{U/L}}$	ratio of uplink command-signal to total power
$P_T/N_0\|_{\mathrm{D/L}}$	ratio of downlink total power to noise spectral density, Hz
$P_C/P_T\|_{\mathrm{D/L}}$	ratio of downlink residual-carrier to total power
$P_R/P_T\|_{\mathrm{D/L}}$	ratio of downlink ranging-signal to total power
$P_D/P_T\|_{\mathrm{D/L}}$	ratio of downlink telemetry to total power
P_R/N_0	ratio of downlink ranging-signal power to noise spectral density, Hz
P_k/P_T	ratio of discrete spectral line power to total power
P_0/P_T	ratio of residual-carrier power to total power
Z	$T_2 \cdot (P_R/N_0)$ in decibels
ρ_ρ	ranging signal-to-noise ratio in transponder's ranging channel
ρ_{cmd}	command-feedthrough signal-to-noise ratio in transponder's ranging channel
B_R	noise-equivalent bandwidth of transponder's ranging channel, Hz
T_1	integration time for range clock, s
T_2	integration time for ambiguity-resolving component, s
f_n	frequency of range component n, Hz
f_{RC}	range-clock frequency, Hz
f_S	S-band carrier frequency, Hz
f_X	X-band carrier frequency, Hz
f_{Ka}	Ka-band carrier frequency, Hz
c	speed of electromagnetic waves in vacuum, m/s
n_{RC}	component number of range clock
n_L	component number of last ambiguity-resolving component
N_C	number of ambiguity-resolving components

ϕ_r	phase deviation of uplink carrier by ranging signal, rad rms
ϕ_{cmd}	phase deviation of uplink carrier by command signal, rad rms
θ_{rs}	phase deviation of downlink carrier by ranging signal (strong signal), rad rms
θ_r	phase deviation of downlink carrier by ranging signal, rad rms
θ_{cmd}	phase deviation of downlink carrier by command feedthrough, rad rms
θ_n	phase deviation of downlink carrier by noise, rad rms
θ_{tlm}	telemetry modulation index, rad
$S_{cmd}(\phi_{cmd})$	suppression factor on uplink due to command
$M_{cmd}(\phi_{cmd})$	modulation factor on uplink for command
$S_{fth}(\theta_{cmd})$	suppression factor on downlink due to command feedthrough
$S_{tlm}(\theta_{tlm})$	suppression factor on downlink due to telemetry
$M_{tlm}(\theta_{tlm})$	modulation factor on downlink for telemetry
P_{acq}	probability of acquisition
σ_ρ	standard deviation of range measurement error, m
σ_τ	standard deviation of two-way delay, s
σ_{RU}	standard deviation of the two-way phase delay, RU
ΔRTLT	change in RTLT over the course of a ranging pass, s

References

1. J. B. Berner, S. H. Bryant, and P. W. Kinman, “Range Measurement as Practiced in the Deep Space Network,” *Proceedings of the IEEE*, Vol. 95, No. 11, November 2007.
2. P. W. Kinman and J. B. Berner, “Two-Way Ranging During Early Mission Phase,” *2003 IEEE Aerospace Conference*, March 8-15, 2003, Big Sky, MT.
3. C. L. Thornton and J. S. Border, *Radiometric Tracking Techniques for Deep-Space Navigation*, Monograph 1 of the *Deep-Space Communications and Navigation Series*, Jet Propulsion Laboratory, Pasadena, CA, 2000.